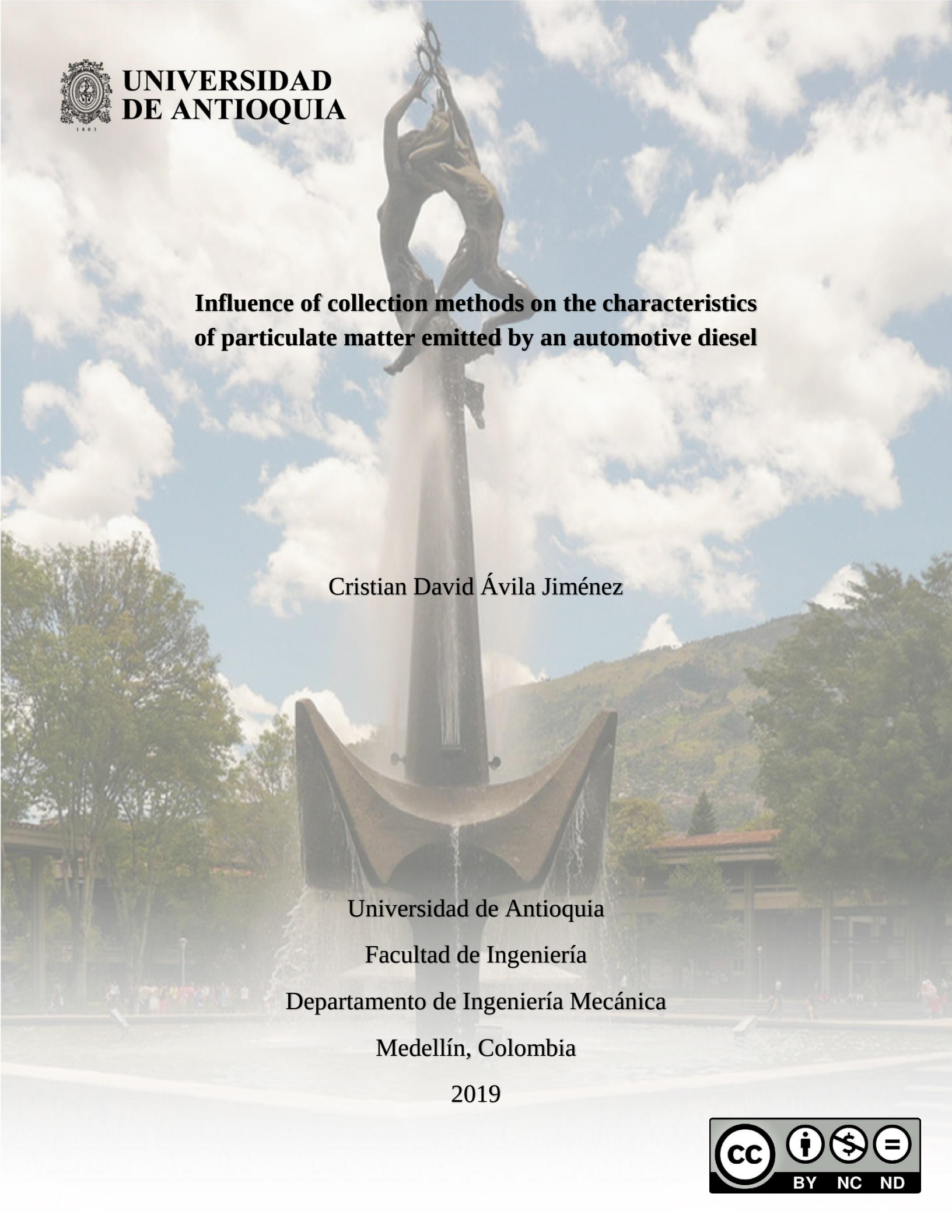

UNIVERSIDAD DE ANTIOQUIA

Influence of collection methods on the characteristics of particulate matter emitted by an automotive diesel

Cristian David Ávila Jiménez

Universidad de Antioquia

Facultad de Ingeniería

Departamento de Ingeniería Mecánica

Medellín, Colombia

2019

UNIVERSIDAD DE ANTIOQUIA

1 8 0 3

Influence of collection methods on the characteristics of particulate matter emitted by an automotive diesel engine

Dissertation for Master's degree in mechanical engineering - Research

Cristian David Ávila Jiménez

Advisor: Dr. Andrés Felipe Agudelo Santamaría
Research Group: GIMEL
Department of Mechanical Engineering
UNIVERSIDAD DE ANTIOQUIA
Medellín, Colombia 2019

Contents

List of Figures

List of Tables

Nomenclature

°C	Celsius Degrees
B10	10% v/v of palm biodiesel and 90% v/v of ULSD fuel
B100	Neat palm biodiesel fuel
CM	Collection methods
CO	Carbon Monoxide
CVS	Constant Volume Sampler
d_{002}	Interlayer distance
D_f	Fractal dimension
DMA	Differential mobility analyzer
DOC	Diesel Oxidative Catalyst
dp_0	Primary particle diameter
DPF	Diesel Particulate Filters
EGR	Exhaust gas recirculation
ELPI	Electrical Low-Pressure Impactor
FL	Fringe length
FS	Fringe Interspace Distance
FT	Fringe tortuosity
FT-IR	Fourier-Transform InfraRed spectroscopy
g	Gamma
HM	High Load Operation Mode
HRTEM	High resolution Transmission Electron Microscopy
KBr	Potassium bromide
kPa	Kilopascals
kV	Kilovolts
L_a	Crystallites length
L_c	Stacking thickness of the crystallites
mA	Milliamperes
$MLRT_{max}$	Maximum loss rate temperature
MM	Medium Load Operation Mode
mm	Millimeters
ms	Milliseconds
MT	Partial dilution mini tunnel
mW	Milliwatts
NOx	Nitrogen Oxides
PAH	Polycyclic aromatic hydrocarbons
PM	Particulate matter

PT	Particle Trap
PTFE	Teflon
RH	Relative Humidity
SMPS	Scanning Mobility Particle Sizer
SOF	Soluble organic fraction
$T_{10\%}$	Temperature at which 10% of the mass is burned
TEM	Transmission Electron Microscopy
T_{exh}	Exhaust gas temperature
TGA	Thermo-Gravimetric Analysis
TP	Thermophoretic Probe
UHC	Unburned Hydrocarbons
VOF	Volatile organic fraction
VP	Vacuum pump
XRD	X-Ray Diffraction spectroscopy

ACKNOWLEDGEMENTS

This study was carried out under the framework of the *Acti-Bio* project funded by the *Federación Nacional de Biocombustibles* (Fedebiocombustibles). I would also like to thank to *Ecopetrol* and *BioD,* fuel manufacturer companies for the fuels supplied. I wish to thank the *Student Instructor Master's* scholarship of the University of Antioquia for the financial support.

I gratefully acknowledge the research group GIMEL for the economic support provided to manufacture the experimental system, conduct the sample analysis, and for the constant academic and emotional support. A very special acknowledge to my colleagues Cristian Ortiz, Manuel Echeverri, Juan Vallejo and Andrés López, for the support provided during the engine and collection tests, and to Marlon Cadrazco and Maria Luisa Botero for the support in the analytical techniques performed and its analysis. I also appreciate the advice and help provided by professor and supervisor Andrés Agudelo.

Finally, I will be eternally grateful with my parents, Nelson Ávila and Nora Jiménez, and my girlfriend Melissa Puerta for the unconditional support along all my academic and professional development.

ABSTRACT

Vehicles powered by diesel engines still represent a significant proportion of the transport fleet in urban areas. The emissions of pollutants, such as particulate matter (PM), from these vehicles have been targeted as possible cause of respiratory diseases and even cancer. For these reasons, the study of PM emitted by automotive engines is of great importance, as well as the impact of rapidly advancing engine technology and after-treatment systems in the characteristics of the emitted PM. Researchers have developed a wide range of methodologies to collect and to characterize the PM emitted by these combustion systems. Nevertheless, there is not a general consensus of the effect that these collection methods may have on the PM morphology, nanostructure, and chemical composition characteristics.

This document presents a study of the effect of different PM collection methods on the properties of PM using diverse characterization techniques. Tests were carried out in an automotive Euro 4 diesel engine installed in a steady-state test rig operating at 2200 rpm and 90Nm, which is highly representative of a medium load of the vehicle running under World-wide harmonized Light duty Test Cycle (WLTC). The PM collection methods used in this work were: vacuum pump (VP) through Teflon filters (PTFE), particle trap (PT) with stainless steel wools, thermophoretic probe (TP) with lacey carbon grids, and partial dilution mini tunnel (MT) with fiberglass filters. The last was included in order to check the impact of the degree of exhaust gases dilution on the morphological, chemical and nanostructure parameters of the PM.

Results showed that for oxidation reactivity and proximate composition through thermogravimetric analysis (TGA), the recommended collecting method, among these mentioned above, is the PT. During the filtering process of the VP, the PM is highly compacted (with higher fractal dimension than the PM from particulate trap) affecting its thermal properties. It was not possible to run TGA tests with fiberglass filters due to the low PM mass collected, and the high uncertainty of the actual PM mass charged in the pan.

Among the collecting methods, the most suitable for chemical functionalities analysis by Fourier-Transform Infrared spectroscopy (FT-IR) was the PT, since this allow obtaining the best signal/noise ratio. With both filters (Teflon and fiberglass), the peak intensity was low, and in addition the sample preparation was more complicated.

With regard to Raman spectroscopy (nanostructure analysis), the most suitable collecting process was the VP with Teflon filters. PT induced in some cases fluorescence anomalies due to the presence of small metallic traces contaminants which forced to take more spots. In view of the costs associated to VP test rig, and the small statistical difference between the results of PT and VP, it is recommended

to use a PT if the VP test rig is not installed. The fiberglass induced fluorescence in most of the cases.

The Transmission Electron Microscopy (TEM) was used to obtain the micrographs of the PM, which allowed to measure the primary particulate diameter and to calculate the fractal dimension of the agglomerates. The High Resolution TEM (HRTEM) was used to determine the fringe length, tortuosity and interspace distance between fringes inside a primary particulate. As expected, the most suitable collection method was the TP, since the PM was not submitted to collisions in filtering media, and modifications during the sample preparation. The fractal dimension was similar for TP and PT, while it was higher with both filter types (Teflon and fiberglass).

For X-Ray Diffraction spectroscopy (XRD) analysis, the most suitable collecting mode was the PT since both filters (Teflon and fiberglass) exhibited signal interference. Small contaminants from the stainless-steel wools are easily localized in the spectra, allowing to delete this from the analysis.

In summary, for thermal, chemical, Raman and XRD analysis it is recommended to collect the PM with PT. For morphological and HRTEM analysis it is recommended to collect the PM through TP. The VP plus Teflon filters mounting system was expensive and did not showed significant differences with respect to particulate trap. The challenge of the PT is to reduce the stainless-steel contamination which mainly affects the XRD spectra.

Key words: *Diesel engines, particulate matter, collection methods, characterization techniques.*

RESUMEN

Los vehículos propulsados por motores diesel aún representan una proporción significativa de la flota de transporte en las zonas urbanas. Las emisiones contaminantes, como el material particulado (PM), de estos vehículos ha sido señalado como posible causa de enfermedades respiratorias e incluso cáncer. Por estas razones, el estudio del PM emitidas por los motores de los automóviles es de gran importancia, así como el impacto del rápido avance de la tecnología de los motores y de los sistemas de postratamiento en las características del PM emitido. Los investigadores han desarrollado una amplia gama de metodologías para recolectar y caracterizar el PM emitido por estos sistemas de combustión. Sin embargo, no existe un consenso general sobre el efecto que estos métodos de recolección pueden tener en la morfología, la nanoestructura y las características de la composición química del PM.

Este documento presenta un estudio del efecto de diferentes métodos de recolección de PM en sus propiedades utilizando diversas técnicas de caracterización. Las pruebas se llevaron a cabo en un motor diesel Euro 4 de automoción instalado en un banco de pruebas de estado estacionario, funcionando a 2200 rpm y 90 Nm, punto que es altamente representativo de una carga media del vehículo que lleva el motor instalado, bajo el World-wide harmonized Light duty Test Cycle (WLTC). Los métodos de recolección de PM utilizados en este trabajo fueron: bomba de vacío (VP) a través de filtros de teflón (PTFE), trampa de partículas (PT) con esponjillas de acero inoxidable, sonda termoforética (TP) con rejillas de Lacey Carbon y mini túnel de dilución parcial (MT) con filtros de fibra de vidrio. El último se incluyó para comprobar el impacto del grado de dilución de los gases de escape en los parámetros morfológicos, químicos y de nanoestructura de la PM.

Los resultados mostraron que, para la reactividad a la oxidación y la composición próxima a través del análisis termogravimétrico (TGA), el método de recolección recomendado, entre los mencionados anteriormente, es la PT. Durante el proceso de filtrado en la VP, el PM está altamente compactado (con una dimensión fractal más alta que el PM de la trampa de partículas) afectando sus propiedades térmicas. No fue posible realizar pruebas TGA con filtros de fibra de vidrio debido a la baja masa de PM recolectada y la alta incertidumbre de la masa real de PM cargada en la bandeja.

Entre los métodos de recolección, el PT fue el más adecuado para el análisis de funcionalidades químicas por espectroscopia infrarroja de transformada de Fourier (FT-IR), ya que este permite obtener la mejor relación señal / ruido. Con ambos filtros (teflón y fibra de vidrio), la intensidad máxima fue baja y, además, la preparación de la muestra fue más complicada.

Con respecto a la espectroscopia Raman (análisis nanoestructural), el proceso de recolección más adecuado fue la VP con filtros de teflón. La PT indujo en algunos casos anomalías de fluorescencia debido a la presencia de pequeñas trazas de metal, contaminantes que obligaron a tomar más puntos. En vista de los costos asociados con la instalación de VP y la pequeña diferencia estadística entre los resultados de PT y VP, se recomienda usar una PT si el sistema de VP no está instalado. La fibra de vidrio indujo fluorescencia en la mayoría de los casos.

La Microscopía Electrónica de Transmisión (TEM) se usó para obtener las micrografías del PM, lo que permitió medir el diámetro de partículas primarias y calcular la dimensión fractal de los aglomerados. Se utilizó el TEM de alta resolución (HRTEM) para determinar la longitud de las capas de grafeno, la tortuosidad y la distancia entre espacios entre las capas de grafeno dentro de una partícula primaria. Como era de esperar, el método de recolección más adecuado fue el TP, ya que el PM no se sometió a colisiones en el medio de filtrado y a modificaciones durante la preparación de la muestra. La dimensión fractal fue similar para TP y PT, mientras que fue mayor con ambos tipos de filtro (teflón y fibra de vidrio).

Para el análisis de espectroscopia de Difracción de Rayos X (XRD), el modo de recolección más adecuado fue el PT, ya que ambos filtros (teflón y fibra de vidrio) mostraron interferencia en la señal. Los pequeños contaminantes de las esponjillas de acero inoxidable se localizan fácilmente en los espectros, lo que permite eliminarlos del análisis.

En resumen, para el análisis térmico, químico, Raman y XRD, se recomienda recolectar el PM con PT. Para el análisis morfológico y HRTEM, se recomienda recolectar el PM a través de TP. El sistema de montaje de los filtros VP más los filtros de teflón es costoso y no mostró diferencias significativas con respecto a la trampa de partículas. El desafío del PT es reducir la contaminación del acero inoxidable que afecta principalmente a los espectros de XRD.

Palabras clave: *Material particulado (PM), técnicas de caracterización, muestreo, motor diésel, métodos de recolección.*

CHAPTER 1

Introduction

INTRODUCTION

The growing need to find substitutes for fossil fuels and to improve their combustion processes have led researchers and manufacturers to produce renewable fuels of all kinds and to develop increasingly complex combustion and after-treatment systems in order to reduce pollutant emissions. These advances, especially in the field of diesel engines, are generally studied from two points of view. The first is the thermal and mechanical performance of the engine, which is directly linked to fuel properties such as heating value and lubricity [1, 2]. The second, is the measurement of pollutant emissions produced by combustion in these systems, focusing on the characterization and normalization of gaseous emissions such as Nitrogen Oxides (NOx), Carbon Monoxide (CO), Unburned Hydrocarbons (UHC), as well as PM [3, 4].The latter, is generally conformed by a core of carbon and traces of metallic ash, coated with condensed organic compounds and sulfates [5].

Currently, there is a great concern about diesel emissions, as these have been considered as carcinogenic agents (A1 according to World Health Organization) [6], being on the same level as asbestos. To reduce PM emissions, several after-treatment systems have been developed, such as *Diesel Particulate Filters* (DPF) . These devices reduce the amount by oxidizing the particles, leading to the emission of smaller particles with larger probabilities of penetrate further in the respiratory tract when breathed. Yao *et al.* [7] and Liu *et al.* [8] performed measurements of PM emitted by diesel engines with after-treatment systems such as *Diesel Oxidative Catalyst* (DOC) and DPF. These authors concluded that after-treatment systems were highly effective in reducing the mass of particles and their organic fraction, but on the other hand, they increased the emission of ultra-fine particles. For these reasons, and for the optimal functioning of these after-treatment systems, it is necessary to perform a correct characterization of the PM produced in combustion in engines.

There are several ways to characterize the PM produced by combustion in diesel engines. For instance, the distribution of particle sizes and the average diameter are measured with equipment that allows the separation of fractions of sizes, such as cyclones, Electrical Low-Pressure Impactor (ELPI), or Scanning Mobility Particle Sizer (SMPS). Another common approach used when comparing fuels or combustion strategies is the measurement of the emission factor of PM (in g/kW-h or g/km). Some of the most common techniques used to characterize the PM collected is characterized are *Thermo-Gravimetric Analysis* (TGA), *Fourier-Transform InfraRed spectroscopy* (FT-IR), *Transmission Electron Microscopy* (TEM), *X-Ray Diffraction spectroscopy* (XRD), and *Raman spectroscopy*. These techniques give information about the reactivity to oxidation, the functional groups, the nanostructure and morphology of PM, respectively.

Although the literature presents numerous works that report collection methods (CM) of PM for its subsequent characterization [5, 9–13], it is not possible to identify the influence of the collection methods used in characterization results.

Therefore, it is important to understand and, when possible, to quantify the influence of the PM collection method in the results of TGA, FT-IR, TEM, XRD spectroscopy, and Raman spectroscopy characterization techniques. This dissertation presents the study of PM emitted by an automotive diesel engine through TGA, FT-IR, TEM, XRD spectroscopy, and Raman spectroscopy. PM was collected by means of vacuum pump, thermophoretic sampling, particulate trap, and a partial dilution mini-tunnel. The effect of the sampling method on the performance of the characterization techniques was established.

CURRENT STATE OF RESEARCH

Until today there are several technological developments in the engines and automobiles fields. Those developments are reached to improve the engine efficiency [14,15] and to reduce the harmful gaseous and particulate emissions. The first one has been achieved through fuel injection systems [16], turbocharging, as well as through advanced combustion strategies, as partially premixed combustion and spark assisted direct injection [17,18]. The second one has been achieved by means of diverse devices like DPF, DOC and the selective catalytic reduction, succeeding high reduction of particulate matter, CO, UHC, and NO_x [3,8,10]. That is why is important to continue the research and development in the area of the internal combustion engines. However, even though all these strategies have been developed, the engines continue to emit polluting emissions, especially PM.

PM emitted from diesel engines/fuels is widely studied worldwide by means of different techniques [19–21]. Boehman and Peng [22], and Bhaskar *et al.* [23] have studied the opacity (smoke meter) of PM produced by diesel engines, using different injection strategies used and the fuel. Boehman and Peng concluded that those strategies are important in the NOx-PM trade-off, and Bhaskar *et al*. concluded that blending 20% v/v of fish oil methyl ester with diesel and using 20% of exhaust gas recirculation (EGR) improves the NOx-PM trade-off. In addition, Jin *et al.* [24], and Mwangi *et al.* [25] carried out tests on different diesel engines, using different fuels to obtain PM for chemical speciation. Jin *et al.* collected the PM by means of a Constant Volume Sampling (CVS) system, and Mwangi *et al.* used the methodology proposed by Chang *et al.* [26], that consisted in filtering the particles using a vacuum pump. These authors concluded that PM produced by diesel combustion contains polycyclic aromatic hydrocarbons (PAH), which are classified as highly carcinogenic.

Zhang *et al.* [27], and Herner *et al.* [28] characterized PM from a single cylinder diesel engine and several diesel vehicles, respectively, by means of the TGA technique. PM was captured using a Mini-Vol low volume particulate sampler and a Constant Volume Sampler (CVS). These authors concluded that PM is mainly constituted by organic compounds, especially sulphates, PAH's and organic carbon. Chandler *et al.* [29], and Wei *et al.* [30] characterized PM from turbocharged diesel engines through TEM. For this characterization, they collected PM directly from the exhaust pipe, by means of thermophoretic sampling and a vacuum pump (VP) (the sample was cooled and diluted). Thermophoretic sampling is widely used because it minimizes the contamination of the collected PM with other constituents from exhaust gases [29,31,32]. Chandler *et al.* highlighted that the mean primary particle diameter (dp_0) of the diesel PM measured by TEM analysis is much smaller than the mobility sizes reported in previous works, measured with devices as the DMA. This is because the DMA measures an equivalent particle size and does not give information about the primary particle size. Both authors also found that PM consists of agglomerates of smaller spherical particles. However, these authors did not make a comparison between thermophoretic sampling and other PM sampling methods.

Some studies show a different trend in the PM oxidation reactivity. On one hand, Al-Qurashi *et al.* [33] found that the PM oxidation reactivity increase with the increase of the EGR from 0 to 20%. In contrast, Li *et al.* [34] and Rohani *et al.* [35] found that the soot reactivity decreases with the increase of the EGR percentage used. Again, besides the different engines used in each study, PM was collected by means of different collection methods. Al-Qurashi *et al.* collect PM in Teflon (PTFE) filters through a VP and then the PM was scrapped from the filters. On the contrary, Li *et al.* diluted the exhaust gases and collect the PM in quartz filters; and Rohani *et al.* capture PM using the methodology proposed by Jung *et al.* [36], that consist in collect PM on a glass surface by means the thermophoretic force. This discrepancy between works highlight that might be it is induced by the collection methods conducted.

Several studies [22,23,32] used biodiesel fuels from different raw materials. There were differences between the PM emitted by diesel fuel and by biodiesel fuel, but only in respect to the particle mass and size. In turn, Salamanca *et al.* [37] conducted studies with neat palm biodiesel fuel (B100). They used a VP and PTFE filters to collect PM emitted by a pre-Euro direct injection diesel engine. This PM was characterized by means of TGA, Raman, and FT-IR. They concluded that the reduction in the particulate matter mass emission was 65% using neat palm biodiesel compared with conventional diesel. Furthermore, the results from TGA and FT-IR showed that the increase in the biodiesel-diesel blend causes changes in the functional groups of the PM. However, the results were not compared with those found with other collection methods.

Agudelo *et al.* [38], Ruiz *et al.* [39], and Soriano *et al.* [40] characterized PM emitted by both different diesel engine technologies and diesel fuels by means of XRD spectroscopy. In these studies, PM was collected by a particle trap filled with stainless-steel wools. Agudelo *et al.* concluded that the condensate compounds present in the volatile organic fraction (VOF) of PM and the $2\theta = 20°$ band from XRD spectra were tightly related. Ruiz *et al.* concluded that the alcohol fumigation and the engine load did not affect the PM nanostructure. Finally, Soriano *et al.* concluded that no clear differences in nanostructure were observed among all soot samples. Again, these XRD results were not compare with those found with other collection methods.

In contrast, Moldanová *et al.* [41] measured the emissions of PM produced by a marine diesel engine, which were collected both, cold with dilution and hot without dilution, using the quartz filters of a SMPS device. They concluded, that there were significant differences in the result of the TGA of PM, depending on the collection method. This difference was observed in the volatile and in the organic carbon fraction of the PM, which were found in greater quantity in the PM collected cold and with dilution. Furthermore, Kasper *et al.* [42] measured two diesel engines: One of marine application and another one of automotive application. This time, they analyzed the result of the particle size distribution by means a SMPS, with the similar sampling installations implemented in reference [41]. Also, they used a Thermodesorber device in the hot stream, that evaporate and absorbed all volatile material. These authors concluded that there were differences in the distribution of particle size, depending on the method of the sampling conditioning: Cold with dilution or hot without volatile material. Furthermore, the authors concluded that the characteristics of PM in their measurements were significantly different for the two engines used, due to the large geometrical, constructive, and operational differences.

In another study that evaluated the influence of the collection method, Ouf *et al.* [43] measured the fractal dimension (D_f) and morphological characteristics of PM collected by two thermophoretic systems (with and without dilution) and two filtering systems, using TEM image analysis. They concluded that filtering systems tend to over-estimate the primary particle diameter and thermophoretic systems were not affected by dilution. However, this study was performed in a diffusion flame burner, and does not represent the complexity of internal combustion engines. Furthermore, there is a discrepancy in the D_f results between some studies. Ruiz *et al.* [39] found D_f values close to 2, while Zhu *et al*. [44] found lower values, close to 1.5. Besides the different engines used in both works, the PM was collected by different collection methods. Ruiz *et al*. used a particle trap filled with stainless-steel wools, while Zhu *et al*. used a thermophoretic probe. Those result reveals that the collection method may have significant effects on PM characterization results.

Increasingly restrictive environmental regulations and the effect of PM collection methods on engine tests duration and costs, have led to great efforts to standardize the collection methodology and the study of PM [5, 12].

There are widely accepted methods for collecting PM emissions. PM mass can be determined by means of cyclones, tapered microbalance, SMPS, ELPI, among others. The most accepted method to measure PM mass emission is through filtering in a dilution tunnel [2,30,45,46]. Authors such as Shah *et al.* [13], Liu *et al.* [8]**,** and Choi and Jiang [45], have managed to implement successful methodologies to collect and measure PM. However, the effort of these authors only went towards measuring PM size distribution, concentration, and total mass.

Currently, there are methodologies established and accepted worldwide for the characterization of diameter, size distribution, total mass, and the ratio of elemental/organic carbon of the PM emitted by engines [5,10,12,47]. But, for some other techniques currently used to characterize the reactivity, functional groups, morphology and nanostructure of PM, such as TGA, FT-IR, TEM, XRD and Raman spectroscopy, there is not a recommended PM collection method [29,30,37].

The literature review shows that, even though that in many studies the PM was collected through methods as PT, VP, MT and TP, there is a lack in the information about the influence of the different collection methods on the PM characteristics. Only one study (Ouf *et al.* [43]) clearly presents results of the PM morphology depending on the methodology used to collect it. Nevertheless, this study was conducted in a combustion system very different to a diesel engine, and only compare thermophoretic and filtering collection methods. That is why this Thesis proposes to evaluate the influence of the collection method of PM emitted by an automotive Euro 4 diesel engine, on the result of characterization techniques such as TGA, FT-IR, TEM, XRD spectroscopy, and Raman spectroscopy. The collection methods to be studied are filtering using a vacuum pump and a partial dilution mini tunnel, particle trap, and thermophoretic sampling. The latter was applied as a base line for the characterization of PM with TEM.

OBJECTIVES

General Objective

To determine the effects of collection methods on the characteristics of particulate matter emitted by a Euro 4 diesel engine, using the typical analytical techniques (TGA, FT-IR, TEM, XRD spectroscopy, and Raman spectroscopy).

Specific Objectives

- To compare particulate matter collection methods: collected amount, times, costs, specifications, results of analytical techniques.
- To select the most appropriate collection method for each characterization technique.
- To determine the combined effect between fuel type and engine operating mode on PM characteristics.

This project did not have external financial support. It was made with resources from the GIMEL group. For this reason, there were economic restrictions that forced us to modify the original specific objectives. In particular, the amount of neat biodiesel available for the tests was limited. Therefore, it was not possible to perform the comparison of the effects of fuel and engine operating mode using all the collection methods (objectives 2 and 3). Nevertheless, this was made with two collection methods (PT and TP). These modifications did not compromise the general objective of this research work. Specific objective 2 was introduced, and specific objective 3 is a combination of the former objectives 2 and 3.

CHAPTER 2

Methodology

METHODOLOGY

Engine test rig and test fuels

An automotive Cummins ISF 2.8L Euro 4 diesel engine (Figure 1) was coupled to an eddy current dynamometer brake (Schenck E90) and tested in two steady-state operating modes. The main characteristics of the engine are listed in Table 1. The engine was equipped with a home-made control and data acquisition system developed in LabView®. This system allows measuring and controlling the engine speed and torque. The engine was also instrumented with several temperature and pressure sensors (before and after of the compressor and turbine, lube oil, fuel, etc.). For the combustion diagnosis, a piezoelectric pressure transducer (Kistler 6056A) coupled to a charge amplifier (Kistler 5011B) was used to measure the instantaneous in-cylinder pressure. Crankshaft rotational speed and instantaneous piston position were determined using an angle encoder (Heidenhain ROD 426), with a resolution of 1024 pulses per revolution. A total of 100 pressure curves, and 3 repetitions were registered at each operating mode to ensure reliability in the combustion diagnosis results. Air consumption was acquired directly from engine´s electronic control unit and fuel consumption was determined with an electronic weight scale (Shimadzu AUW120D ± 0.01 mg).

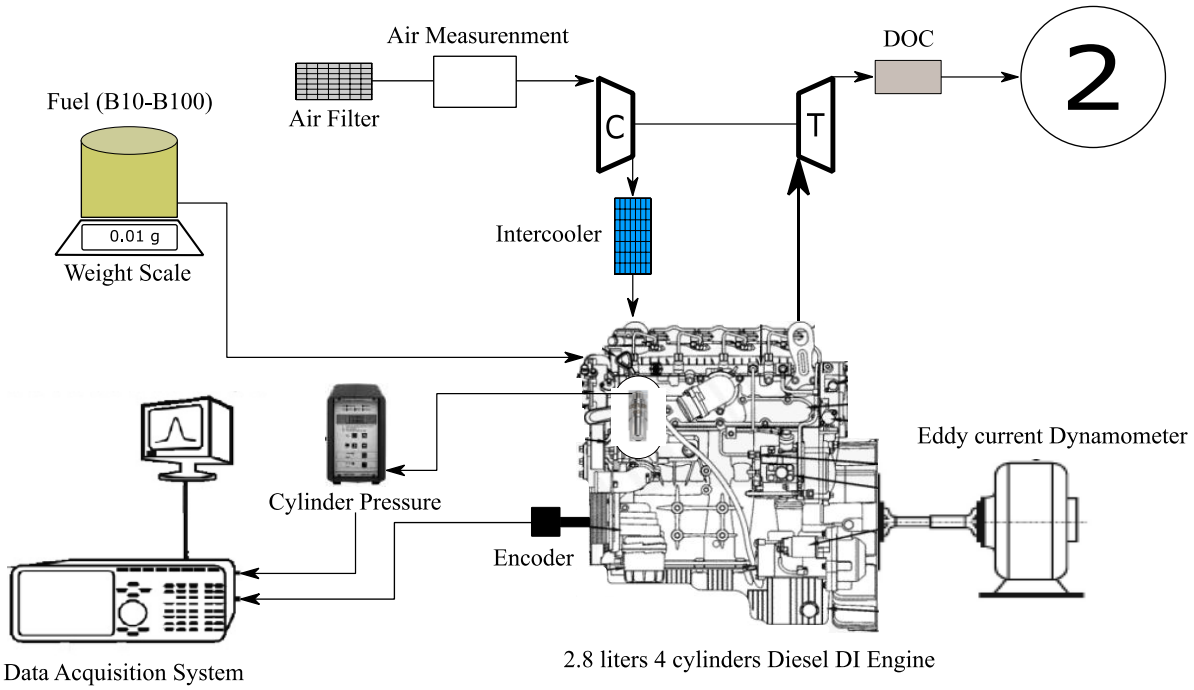

Figure 1. *Engine experimental setup.*

Table 1. *Engine specifications.*

Type	Cummins ISF 2.8, 4 stroke, direct injection
Configuration	4 cylinders in line
Bore & Stroke [mm]	94 x 100
Displacement [L]	2.8
Compression ratio	17.5:1
Power [kW @ min^{-1}]	120 @ 3600
Peak Torque [Nm @ min^{-1}]	360 @ 1800

Engine operating modes correspond to medium (MM, 2200 min^{-1} – 90 Nm) and high (HM, 2800 min^{-1} – 80 Nm) vehicle load. These modes were obtained by means of longitudinal dynamics analysis and the *Vehicular Specific Power* methodology [48]**,** applied to the vehicle that has the engine installed (Foton Tunland). This procedure was applied using the *World-wide harmonized Light duty Test Cycle* (WLTC). These modes were selected because their stability and repeatability during operation in the test rig, and because they are representative of urban driving conditions.

To evaluate the effect of the fuel oxygen content, two different fuels were tested: B10 (10% v/v of palm biodiesel and 90% v/v of ULSD fuel) and B100 (neat palm biodiesel fuel). The main physicochemical properties of tested fuels are shown in Table 2. B100 was supplied by *BioD* and ULSD was supplied by *Ecopetrol S.A*. Both companies are Colombian fuel manufacturers.

Table 2. *Fuel properties*

Fuel	B10	B100	Standard
Chemical formula	$C_{14.95}H_{29.25}0_{0.15}$	$C_{18.01}H_{34.85}0_2$	Calculated
Molecular weight [g/mol]	211.508	282.921	Calculated
Lower heating value [kJ/kg]	42,119	37,329	ASTM D240
Density 15°C [kg/m]	860.87	874.8	ASTM D4052-15
Derivative Cetane number	47.9	69	ASTM D7110
Kinematic viscosity 40 °C [cSt]	-	4.657	ASTM D445-15a
Oxygen [%w/w]	1.13	11.31	Calculated

Collection methods and Sampling procedure

Figure 2 presents the PM collection methods used in this work.

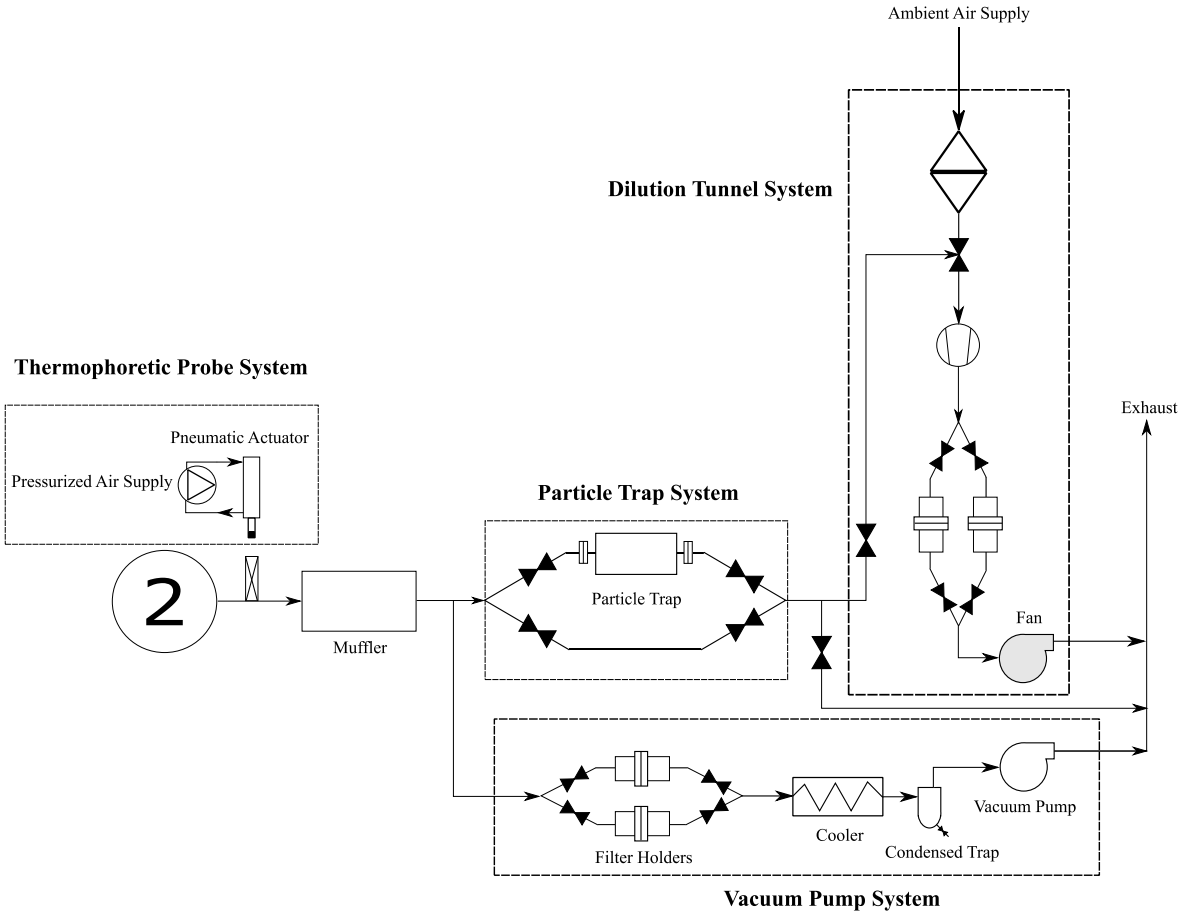

Figure 2. *PM collection methods setup.*

Thermophoretic probe (TP)

A TEM grid holder coupled to a pneumatic actuator is used to collect particles at the engine exhaust by means of the thermophoretic effect, which is the mass transfer produced by a temperature gradient between a cold surface and a hot flux of particles [49]. Sampling grids were special *Ted-Pella* carbon-supported, 3.05 mm diameter TEM grids (300 mesh Lacey-carbon coated standard square copper grids). Each sampling was made with double insertion, each one with a residence time of 200 ms, and a period of 20 s was allowed between insertions. A picture of the TP collection device implemented is shown in Figure 3. The device is conformed by a bistable pneumatic valve, to commute the air supply; a pull-down circuit, to reference the ground; and a pneumatic actuator, which produce the linear necessary movement to introduce and extract the grid into the exhaust pipe. Finally, to temporize the residence time and control all the process, two limit

switches sensors were connected to a Micro Programmable Logic Controller (PLC) Controllino®. This device is programmable by Arduino® and works as an industrial PLC. The TP method was only applied as a baseline for the characterization of PM by TEM image analysis, given that the collected amount of PM with this method is significantly less compared to the other three collection methods.

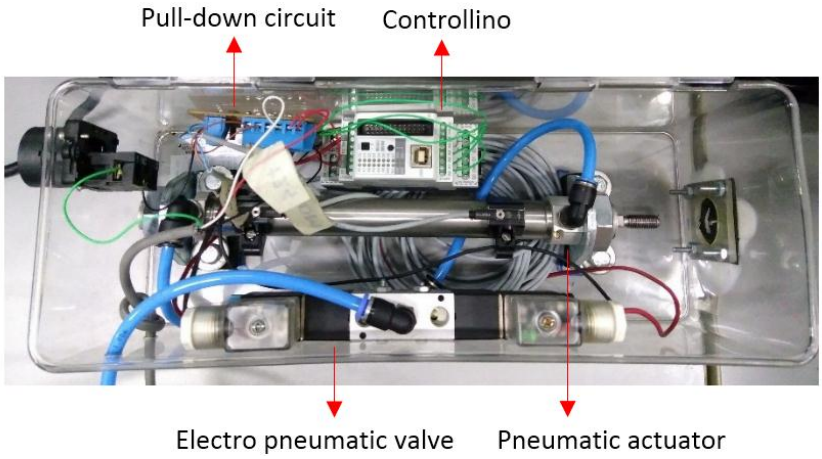

Figure 3. *TP collection device.*

Particle trap (PT)

This is a cylindrical cavity filled with stainless-steel wools, which was installed in the exhaust pipe, right after the muffler. This method allows to collect higher amounts of PM compared to other methods, and it has been used in several works [38–40] Two pressure sensors were installed, one before and one after the PT, to guarantee a maximum pressure drop of around 8 kPa during PM collection. B10 and B100 fuels were tested for 2 and 5 h, respectively, in order to collect enough PM with this system.

Vacuum pump (VP)

A vacuum pump (Edwards RV 3) is used to collect PM hot samples without dilution on PTFE filters (ANPEL CM0312 Laboratory Technologies, porosity $0.22\ \mu m$). Tests for each filter lasted about 15 min, in order to collect enough PM. 5 filters were used for each fuel and engine operating mode (one for each characterization technique). A picture of the VP collection device implemented is shown in Figure 4. To be more efficient, the system has two sample sides, commuted by means of four high temperature valves, to prepare the next sample while one side is collecting PM. Furthermore, to protect the integrity of the vacuum pump, a water-cooled chiller and a condensate drainer were installed in the system. Those devices allow to reduce the gases temperature below 40°C and extract the possible condensates, respectively, preventing the entering of the high temperature gases and corrosive products into the pump.

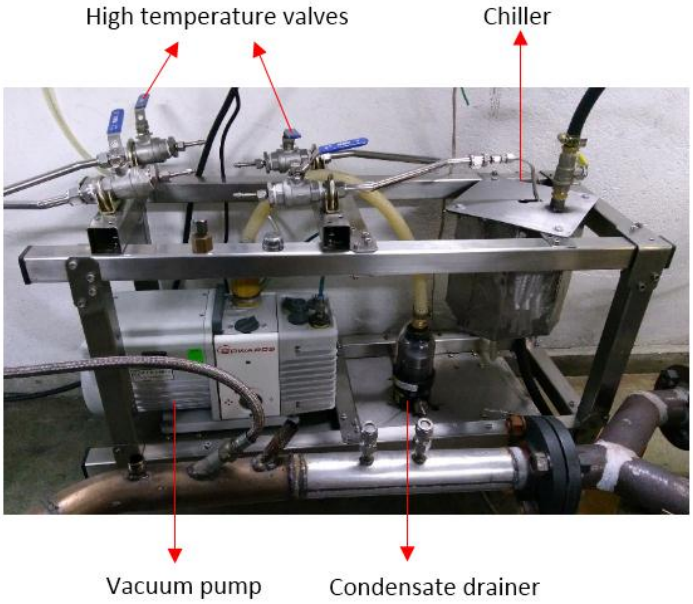

Figure 4. *VP collection device.*

Partial dilution mini tunnel (MT)

PM samples were collected cooled and diluted onto fiberglass filters (ADVANTEC GC 50, porosity $0.50\ \mu m$) using a partial dilution mini tunnel installed at the exit of the exhaust pipe. The dilution ratio (4:1) was calibrated by means of NO_x concentration (in ppm). This ratio is measured before and after the dilution system. PM was collected using the same time that was used during the collection process in the VP system, in order to compare both methods.

Analytical techniques

Before and after the PM collection, PTFE and fiberglass filters were conditioned and weighted in a climatic chamber for 24 hours. The temperature and relative humidity were $22\ \pm 2\ °C$ and $45\ \pm 5\ RH$, respectively. Once PM was collected in the filters using the VP and MT collection methods, gravimetric measurements of PM were performed, using a high precision weight scale Shimadzu AUW120D (± 0.01 mg). Furthermore, after PM was collected through the previous four collection methods, it was characterized through the following five material characterization techniques.

Thermo-Gravimetric Analysis (TGA)

The measurement is based on the mass loss of a material exposed to a heating program and to a type of atmosphere (reactive or inert). This technique allows to calculate the reactivity to oxidation of the particles, and to estimate their kinetic parameters of reaction. Soot oxidation reactivity and the proximal analysis were obtained through the heating program proposed by Soriano *et al.* [40]. The experiments were carried out in a TA Instruments Q50 thermogravimetric analyzer, and the total flow rate of gases was adjusted at 100 mL min^{-1} during each test. For the powder soot samples, a minimum of 3.2 mg was loaded into the alumina pan, while a minimum of 2 mg of PM, recovered from the PFTE filters, was loaded. For the PM in the fiberglass filters, the approach developed by Lapuerta *et.al* [50] was adopted. Before this work, a repeatability test of the TGA equipment was conducted using diesel soot. Results showed a standard deviation of 1.3 °C for maximum loss rate temperature ($MLRT_{max}$) [40]. In this work, the parameters to compare the thermal performance of the PM are the $MLRT_{max}$ and the temperature at which 10% of the mass is burned ($T_{10\%}$).

Fourier-Transform Infrared Spectrometry (FT-IR)

It is based on the measurement of molecular vibrations in a material, induced by an infrared beam of light, allowing to know the molecular "trace" of the material measured. Through this technique, it is possible to know the chemical compounds present in the PM surface. A potassium bromide (KBr) pellet was prepared in 1 wt % of powder PM sample (from PT) and in 0.5 wt % of PM sample from PTFE or fiberglass filters (from VP and MT, respectively) for qualitative FT-IR analysis. For this, PM was sonicated in dichloromethane for 20 min to obtain the soluble organic fraction (SOF), and then the extract was filtered. After that, KBr pellets were dried at 100°C in a furnace for 6 hours. Each spectrum was the result of the accumulation of 32 scans. A Nicolet Magna 560 spectrometer was used with a Mercury cadmium telluride (MCT/A) detector. It was operated in a wavenumber range of 600-4000 cm^{-1}. To attain reliable comparison of the absorption peaks, each spectrum was normalized by the 2925 cm^{-1} aliphatic peak as proposed by Mckinnon *et al.* [51] and Santamaría *et al*. [52]. Three replicates of each sample were taken to estimate repeatability of the method. In general, the uncertainty in the IR measurements was less than 5%.

Transmission Electron Microscopy (TEM)

This technique is based on the reception of a beam of electrons that cross an ultra-fine sample. This analysis technique allows determining the structure of different materials. Furthermore, it allows knowing and measuring the morphology and nanostructure of the PM. Morphological (fractal dimension) and nanostructural (fringe length (FL), fringe interspace distance (FS), and fringe tortuosity (FT)) analysis were conducted through the methodologies proposed by Lapuerta *et al.* [53]**,** and Botero *et al.* [54] and Cadrazco *et al.* [55], respectively. Low and high-resolution images were taken using a FEI Tecnai G^2 F20 Super-Twin transmission electron microscope with an operating voltage of 200 kV.

More than 5 TEM images were used for fractal analysis using 29,000 x magnification. At least 150 primary particles were measured for primary particle diameter and its distribution using the previous magnification. Finally, more than 4 HRTEM images were used for nanostructural analysis using 490,000 x magnification.

Collected PM through PT, VP and MT were dispersed in ethanol by means of an ultrasonic bath. PM from PT (as a powder) was directly dispersed, while PM from VP was scraped from the PTFE filter, and then it was dispersed. Further, PM from MT was dispersed by cutting and sonicated the fiberglass filter directly in ethanol. Every dispersion was performed for 20 min. Finally, for each collection method, a dispersed drop was placed in a Lacey Carbon TEM grid and heated for 12 h before the analysis. On the other hand, the TEM grid from TP was used directly in the analysis without any treatment.

X-Ray Diffraction spectroscopy

It is based on the coherent scattering of the X-ray beam by the measured matter and on the constructive interference of waves that are in phase, and those that are dispersed in certain directions of space. This technique allows determining the lattice parameters and crystallite size (nanostructure) of PM samples. The above parameters were determined through XRD spectra recorded in a Panalytical Xpert Pro MPD, with a standby of 30 kV to 10 mA, according with the approach of Iwashita *et al.* [56]. The test was performed at 45 kV and at 40 mA. A beam mask of 10 mm with a slit of 0.5°, and a copper radiation source were used. A scan speed of 0.034105 (°/s) at a step of 0.0263° were fixed between 10° and 60°. The PM samples were supported directly in a zero-background holder, either powder (from PT) or in filter (from VP and MT). The lattice parameters of the interlayer distance (d_{002}), the crystallites length (L_a) and stacking thickness of the crystallites (L_c) were determined based on the Bragg's law and on the Scherrer equation [57], and by deconvoluting the diffractogram as is proposed by [39].

Raman spectroscopy

It is based on the analysis of monochromatic light scattered by a material, allowing its nanostructural recognition. It enables to identify the state of graphitization (the order of graphene layers) and the nanostructural irregularities. A LabRam HR Horiba microscope system provided with a 632.8 nm He/Ne laser excitation source was used to register Raman spectra. PM from PT was placed in a glass sample holder for the analysis. PM from VP and MT were measured directly from the filters. All PM samples were in the spectral range of 500-2600 cm^{-1} with a 50x magnification objective. An exposition time of 20 s and a source power of 0.17 mW were used to avoid sample burn-off [58]. Four curve-fitting methods were employed for first-order Raman spectra as proposed by [59]. Three Lorentzian functions, one for the G band around 1605 cm^{-1}, and two for the defect bands D1 and D4, located around 1340 and 1130 cm^{-1}, respectively. Finally, one Gaussian function was used for the band D3, around 1534 cm^{-1}. No appreciable D2

band, located around 1620 cm^{-1} was exhibited by any sample. Five different spots were analyzed and averaged for each sample.
It is important to highlight that the PM collected by means of PT, VP, and MT were characterized by means of the four characterization techniques mentioned. However, the PM from the TP method was used only as a base line for the characterization of PM by the TEM technique.

Finally, a statistical random uncertainty (u_A) and coefficient of variance (COV) analysis were performed (Figure A3. 1.), in order to guarantee the reliability of the experimental measurements. It was found that the u_A was low, and that the COV was below 4% all measured variables, which give reliability to the data from the experimental test rig.

Experimental matrix

To achieve the specific objectives, the next procedure was followed:

- First to all, PM was collected using the 4 collection methods mentioned (PT, VP, MT and TP) in MM operation mode, using B10 fuel only. This is justified for the higher soot emission of B10 compared with B100 fuel, and for the fuel availability. PM collected through PT was characterized by all the techniques mentioned. PM collected through VP was characterized by TGA, FT-IR, Raman and XRD. Characterization of the VP sample was not possible by TEM and HRTEM because there was contamination from PTFE filters. PM from MT system was characterized by all the techniques excepts by TGA, due to the low mass collected into the filters and the uncertainties in the PM mass charged into the crucible. Finally, PM collected through TP was only characterized by TEM and HRTEM. Table 3 summarized the experimental campaign used to compare the collection methods and the characterization results. The red crosses indicate that the PM was collected and tested in the corresponded characterization technique. The blue crosses indicate that the PM was collected but the characterization did not present any information.

Table 3. *PM collection matrix to determine the difference between collection methods*

MM - B10						
CM \ CT	TGA	FTIR	Raman	TEM	HRTEM	XRD
PT	+	+	+	+	+	+
VP	+	+	+	+	+	+
MT	+	+	+	+	+	+
TP				+	+	

- To compare the result of the characterization techniques, regarding the fuel used (B10 or B100), or the engine operation mode (MM or HM) only the PM collected using the PT were characterized by means of TGA, FT-IR, Raman, and the PM using the TP were characterized by means of TEM and HRTEM.

Table 4. *PM collection matrix to compare fuels and engine operating modes*

MM and HM - B10 and B100					
CM \ CT	TGA	FTIR	Raman	TEM	HRTEM
PT	+	+	+		
TP				+	+

CHAPTER 3

Results and Discussion

RESULTS AND DISCUSSION

This chapter presents the main results from the PM collection and its characterization, as well as the discussions related to the combined effect of the PM collection methods and the characterization techniques. The chapter has two sections, the first one is the comparison of the results among collection methods, and the second one is the comparison among engine operation modes and fuels used in this work.

Effect of the collection methods

For both fuels and both engine operation modes, PM was collected by means of PTFE filters (VP system) and fiberglass filters (MT system). Also, for morphological and nanostructural analysis, PM was collected in TEM grids by means of a TP. The filters were weighted into a controlled climatic chamber before and after the tests to determine the amount of PM collected. Figure 5 shows the PM mass emission from the weighted filters, using a collection time of 15 minutes for each sample. As was expected, the higher PM mass was collected with B10 fuel, in both engine operation modes, due to its higher sooting level compared to B100 fuel [37,60–62]. Besides, the higher amount of PM was collected by means of filtering in VP system. It is important to note that collected mass of PM is not enough for some analytical techniques such as TGA. The mass collected by PT is not plotted due to (it) was always higher than 100 mg. This quantity is enough to conduct all the characterizations.

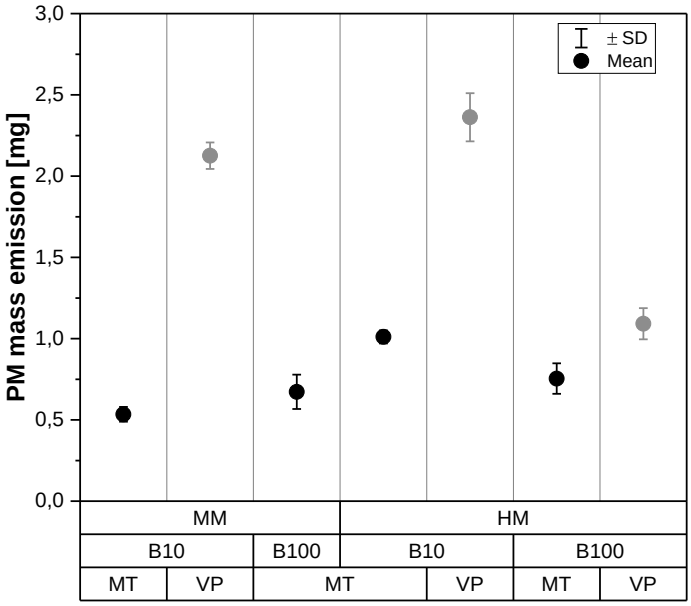

Figure 5. *PM mass emission from filters*

This information is important to determine how many filters are necessary to collect the mass required to conduct several analyses, depending on the engine load, fuel type, and collection method used. This result is relevant for future research campaigns in the same system used in this work.

As shown in Figure 6 (left), the collection method used has a significant effect on the soot oxidation reactivity (from TGA data). It can be observed that PM from PT is more reactive than PM from VP. Soot oxidation from the filter of MT did not present relevant information. The sample preparation for this collection method implies significant uncertainties on the PM mass loaded to the TGA. Furthermore, the PM mass collected in each filter was not enough to conduct a TGA analysis, even if a whole filter was loaded into the equipment. For these reasons, the MT collection method is not adequate for TGA analysis.

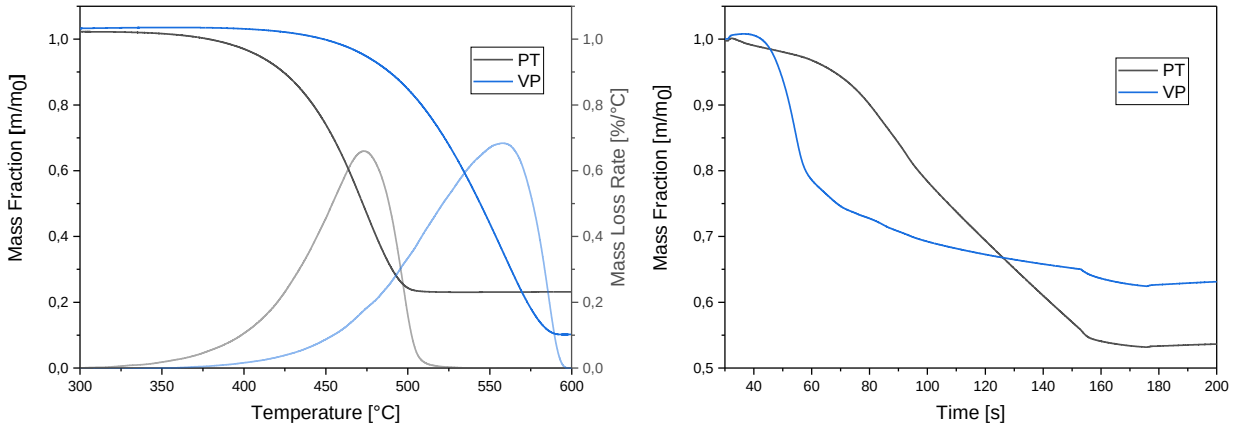

Figure 6. *Mass loss, mass loss rate (left) and VOF mass loss rate (right) for PM of MM-B10*

Oxidation reactivity of particulate matter has been explained usually through the specific surface area of the primary particles [57], the active surface area [38], or by the surface chemical compounds [40,63]. Table 3 presents $MLRT_{max}$ and $T_{10\%}$ for PT and VP samples. Both parameters are lower for PM from PT than from VP. This implies an earlier oxidation reactivity for PT sample. This result might be due to the higher VOF of the PT sample compared to the VP sample (Figure 6 right and Table 3). The longer collection time of the PM in the PT collection method (around 1 hour vs. 15 minutes for VP), may result in higher VOF adsorption by the PM, as can be seen in Table 3. The higher the VOF devolatilized in the PM, the higher the active surface area; therefore, the higher the oxidation rate [39]. Furthermore, as Sánchez-Valdepeñas presents [64], the PM sample collected through VP collection method undergoes a “compaction” process due to the pressure drop in the filtering process. This leads to a decrease in the porosity of the PM, which reduces the possibility that oxygen reaches the sample during the oxidation analysis in TGA. For these reasons, it is recommended to collect PM by means of a PT to perform TGA analysis, provided that the collection time is reduced and the possible metallic contamination from the wools be minimized.

Table 5. *Oxidation temperatures and Proximate analysis depending on CM*

Collection Method	Oxidation Temperatures		Proximate Analysis		
	$MLRT_{max}$ [°C]	$T_{10\%}$ [°C]	Ash [%]	VOF [%]	Carbon [%]
PT	473.3	424.0	12.5	46.1	41.4
VP	557.7	488.8	6.5	36.7	56.8

Chemical functional groups in the surface of PM, from FT-IR analysis, are presented in Figure 7. There are several differences in the absorbance, depending on the collection method.

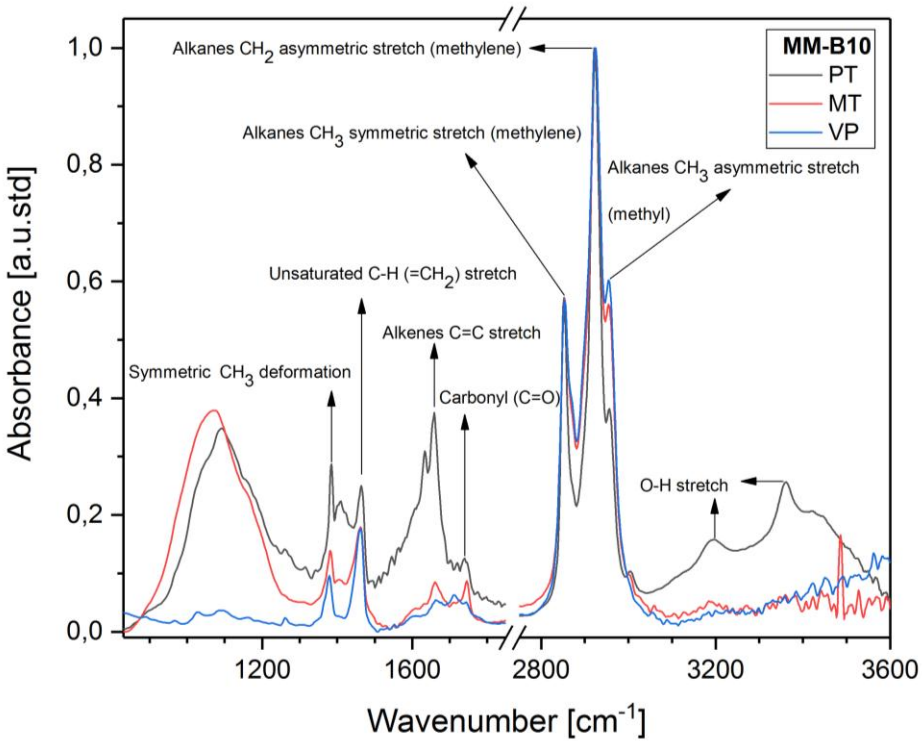

Figure 7. *FT-IR absorbance for PM of MM-B10*

These differences are significant at around 1380 cm^{-1} (symmetric CH_3 deformation [52]), 1460 cm^{-1} (Unsaturated $=CH_2$ stretch [65]), 1640 cm^{-1} (C=C stretch [66]), and 3100-3500 cm^{-1} (O-H stretch [63]). Although PT and VP samples were collected at $T_{Exh} \approx 311.76\,°C \pm 1.9\,°C$ (see Figure A3.2), and without dilution, the longer collection time of PM in the PT could have led to adsorption of VOF and to partial passive oxidation**.** As found by Ishiguro *et al.* [66] the more oxidized the PM sample is, the bigger the peak 1640 cm^{-1} is. This supports the hypothesis that PM from PT was partially oxidized in a passive fashion. In addition, PM from PT shows more O-H absorbance, which is likely due to H_2O

condensation in its surface during the cooling of the PT (for a period of 6 hours) and during the extraction process from the stainless-steel wools. On the other hand, the samples from VP and MT did not present moisture gain, because of the filter conditioning process.

There are two points of view that must be considered to select which collection method is more appropriate to conduct FT-IR analysis. From FT-IR results, the more suitable collection method is that which provides PM with the more defined absorbance peaks, because this will allow to observe more accurately the differences between samples. As is stated by Santamaría *et al.* [52], infrared groups present in the PM are mainly due to compounds from the SOF, and Lapuerta *et al.* [50] explain that SOF content is proportional to the VOF content. Based on proximate analysis (Table 3), this implies that both PT and VP could be adequate collection methods to perform FT-IR analysis. Nevertheless, the PM mass collected with VP system must be higher than the mass collected in this study, in order to obtain a higher amount of SOF after the extraction. On the other hand, the collection time of PM in the PT must be shorter than the time used in this work, to avoid passive oxidation. Therefore, from the IR results it is recommended to collect PM by means of a PT, provided that the collection time is shorter than that used in this work.

Regarding the sample preparation procedure, there are differences in the manufacturing of the KBr pellets. It is important to note that, for qualitative FT-IR analysis, the quantity of PM used in the preparation of the pellets must be the same. PM from the filters is difficult to extract, and it is not possible to extract completely PM mass (either by scrapping the PTFE filter or by sonicating directly the fiberglass filter). For these reasons, it is considered more appropriate to use PM from PT to carry out this chemical analysis, due to its easier manipulation in the weighing and extraction processes, as compared to the other collection methods. In addition, it was found that possible sample contamination by this collection method does not affect the results of this analytical technique.

Figure 8 presents the Raman spectra from PM collected using PT, MT and VP methods. The spectra obtained from PT and VP are similar. On the other hand, the deconvoluted spectra from MT presents differences in all bands, particularly in the region of the D4 band. The distortion evidenced for MT spectrum (see 800-1200 cm^{-1} in the Raman shift) is likely due to fluorescence phenomenon caused by the fiberglass filter.

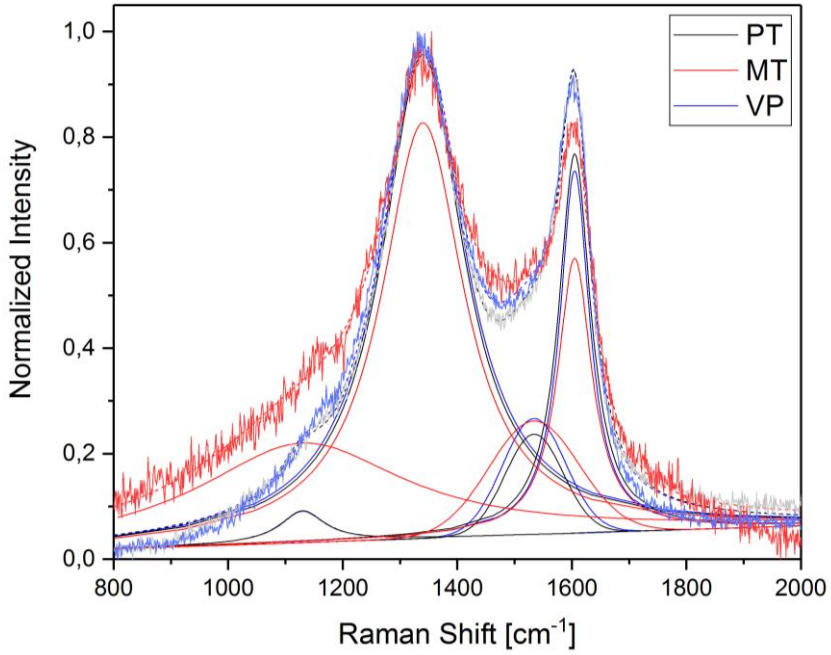

Figure 8. *Typical Raman spectra for PM of MM-B10*

Figures 9 and 10 display the area and intensity ratios, respectively. Given that results of the deconvolutions from MT spectra are altered by the interference of the fluorescence (which leads to high standard deviations in A_{D4}/A_G ratio), this collection method is not recommended for evaluating soot nanostructure using Raman spectroscopy. Results from PT and VP show no differences in the calculated ratios (except for A_{D1}/A_G ratio), suggesting that collection method does not affect soot nanostructure.

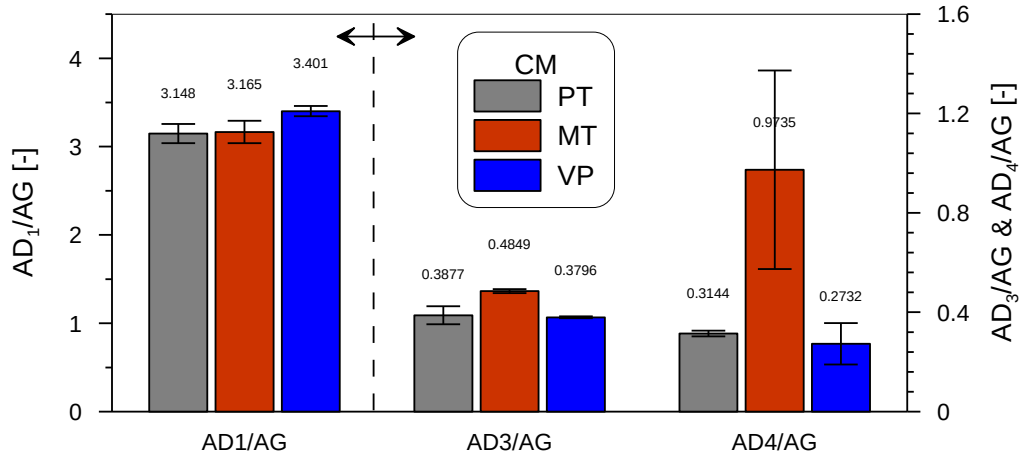

Figure 9. *Raman peaks areas for PM of MM-B10*

Regarding to Raman experiments, the test procedure must be discussed. On one hand, the measurements with PM from PT takes much effort to find an appropriate zone in the sample, due to some metallic contamination of the sample by the wools and to the irregular distribution of the powder. In contrast, the measurements with PM from VP is faster and easier, given that there is no contamination, and the background filter does not interfere with the spectrum. Consequently, it is recommended to collect PM in PTFE filters by means of a VP system, in order to conduct Raman spectroscopy analysis. Nevertheless, in view of the costs associated to VP test rig, and the small statistical difference between the results of PT and VP, it is recommended to use a PT if the VP test rig is not installed.

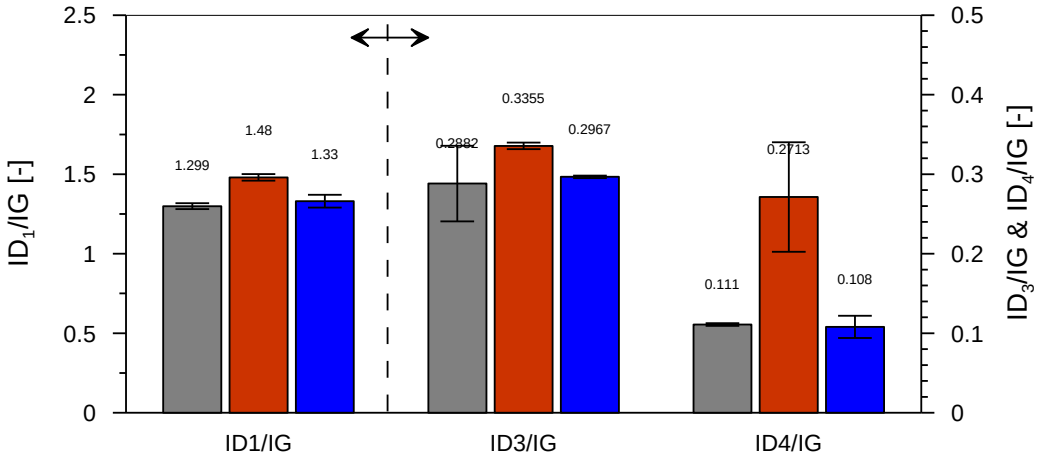

Figure 10. *Raman peaks intensity for PM of MM-B10*

Figure 11 presents the histograms of the primary particle diameter from TEM micrographs (Figure A3.4), as well as the corresponding log-normal distributions, which were fitted to data using statistical goodness of fit tests. As can be seen, although the values of the mode are similar, TP captures higher primary particles than the other collection methods. Also, the expected value for each distribution and its 95% of confident interval is depicted in Figure 12. Although there is not statistical difference between the results, the particles collected by means of TP include higher diameters than the particles collected by the other methods. This could be explained by the nature of the thermophoretic force, which is directly proportional to the particle radius [57]. Another explanation for lower dp_0 values for PM from PT, VP and MT collection methods might be the higher residence time of PM into the exhaust stream, allowing for surface oxidation [67]. However, the values obtained for dp_0 in all the cases are in agreement with the values found in other studies for PM from diesel fuel [44,68,69], which is quite similar in chemical and physical characteristics to the B10 fuel used in this work.

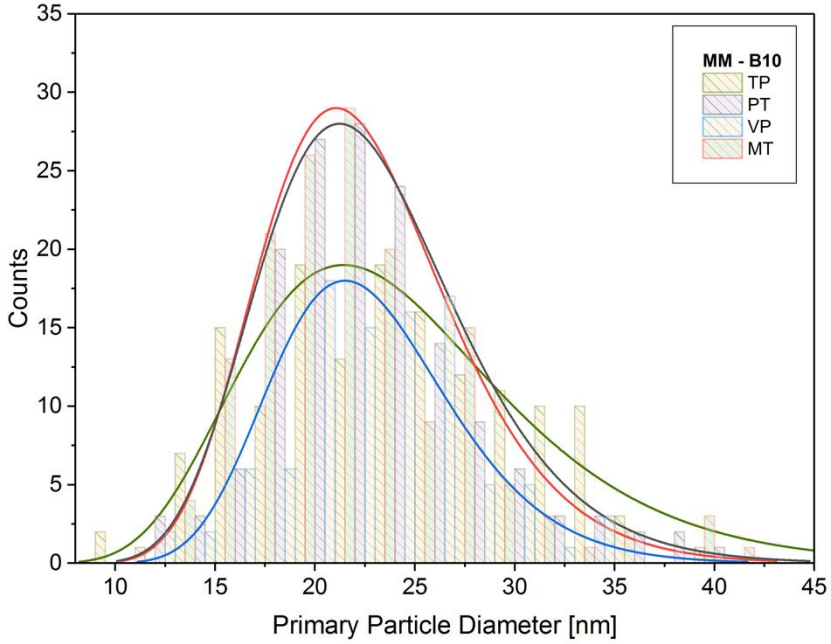

Figure 11. *Primary particle diameter distribution for PM of MM-B10 from TEM micrographs*

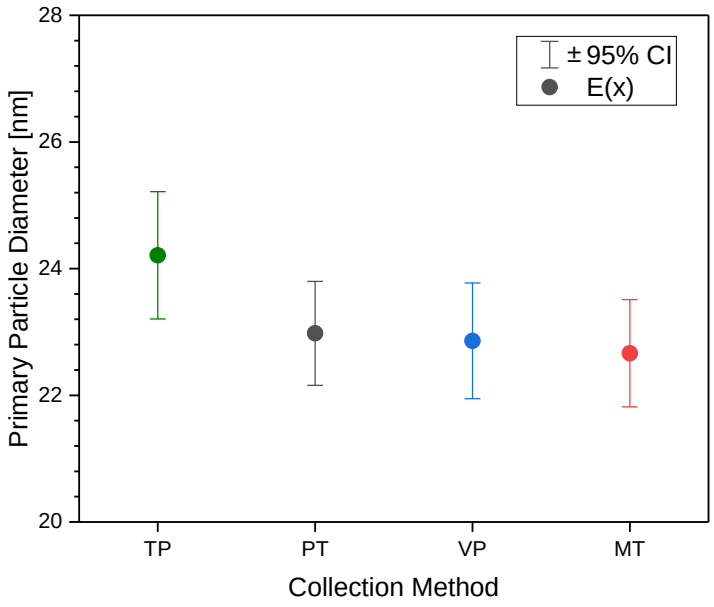

Figure 12. *Expected primary particle diameter for PM of MM-B10 from TEM micrographs*

Regarding the test procedure, the preparation of TEM grids to conduct TEM and HRTEM analysis is important. While PM from PT, VP and MT must be dissolved into ethanol in a sonication bath, and then suspended into a grid, PM from TP is essentially ready to carry out the micrographs. This time saving from sample preparation procedures allows to a

more effective use of available time, which results is a higher number of micrographs. For these reasons, it is recommended to use a TP to collect PM for TEM and HRTEM analysis.

Figure 13 presents the fractal dimension (D_f) of the agglomerates for PM from all the collection methods used. There is a significant trend to increase the D_f downstream of the exhaust pipe. This result is in agreement with Giechaskiel *et al.* [70], who show the growth of the PM aggregates through the exhaust pipe and the CVS device. Also, filtering PM, either in fiberglass or PTFE filters, might increase the agglomeration process, i.e., the D_f. This is also in accordance with Lapuerta *et al.* [71], who stated that the differences observed in D_f may be attributed to the temperature of sampling procedure. In this case, again, it is recommended to capture PM using a TP and full-film TEM grids. Additionally, the TP collection method avoids the PM aggregate morphological modification, which might occur into the filtering media and during the TEM sample preparation process (sonication bath and grid impingement), as is mentioned by Guerrero *et al.* [72]. This is in agreement with the information presented in Figures 13 and A3.5.

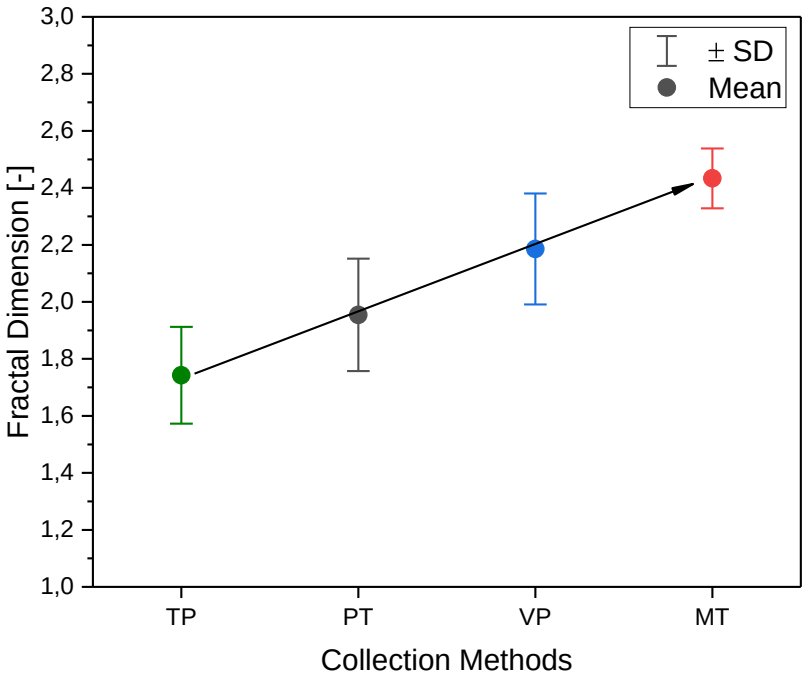

Figure 13. *Fractal dimension for PM of MM-B10 from TEM micrographs*

Figures 14, 15 and 16 present the results from the nanostructural parameters: fringe length, fringe tortuosity, and fringe interspace distance, respectively. Those results were obtained from the HRTEM micrographs, using the image processing methodology proposed by Cadrazco *et al.* [55]. It was not possible to obtain viable high-resolution images from VP filters. Therefore, there are not nanostructural results for PM from that

collection method. This might be due to sample contamination by PTFE during the extraction and sonication process, as is presented in Figure A3.5 (MM-B10-VP). The following results are in good agreement with the results presented by Savic *et al.* [73], whose experiments were carried out in a turbocharged Euro 4 engine. This engine meets the same emission standard as the one used in this work.

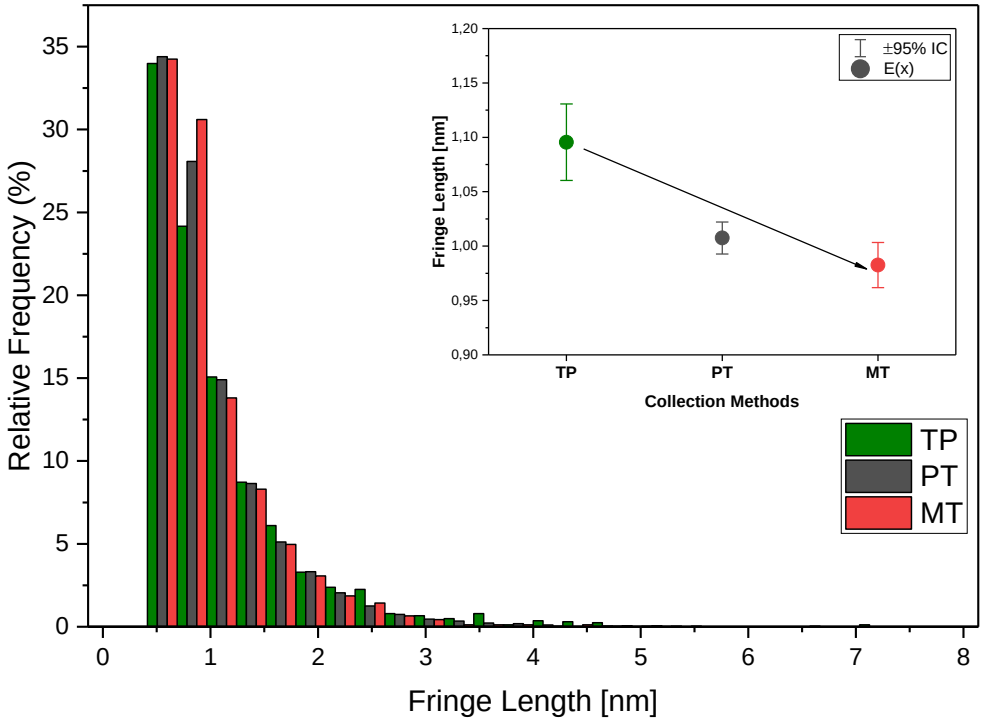

Figure 14. *Relative frequency of fringe length for PM of MM-B10 from HRTEM micrographs*

There is a relationship among the results from Figures 12, 14 and 15. Although there are no statistical differences in the primary particle diameter, while both dp_0 and FL decrease, the FT increases. The formation and growth processes of the primary particles might explain this trend. When the primary particle diameter increases, the new graphene layers in the particle outer side could be longer and flatter than the layers in its core. For this hypothesis to be fulfilled, the FS must not vary, while the fringe length increases, as was found by Aso *et al.* [74]. As Figure 16 shows, there is not difference in the FS among the collection methods used. This trend is consistent with the results observed in the work conducted by Lu *et al.* [75].

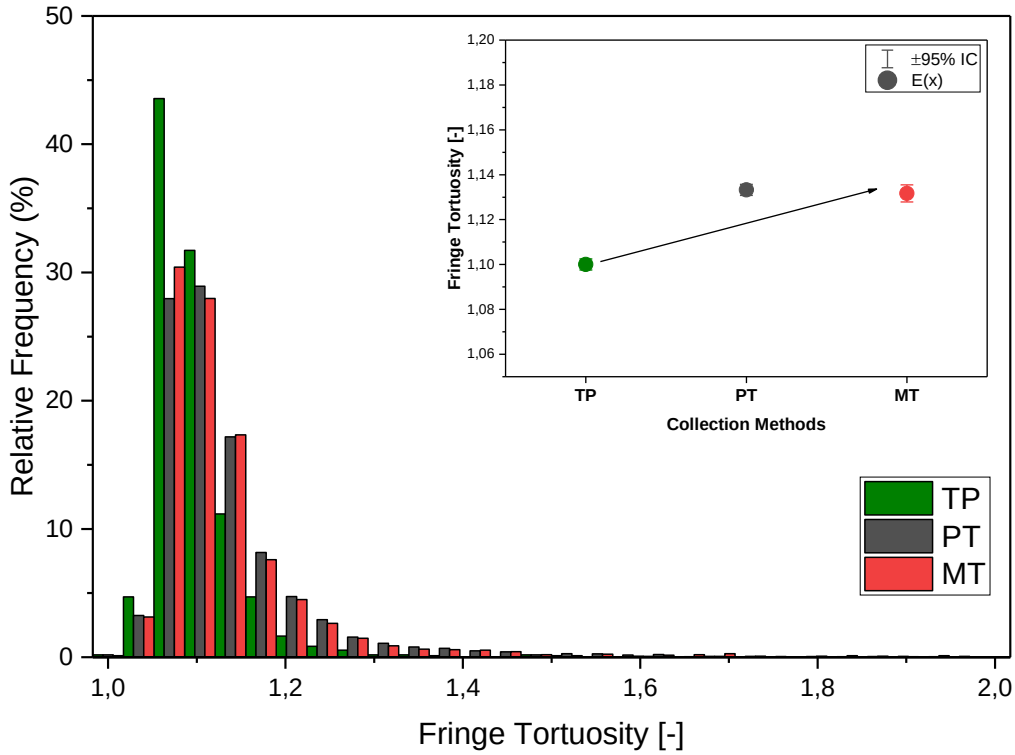

Figure 15. *Relative frequency of fringe tortuosity for PM of MM-B10 from HRTEM micrographs*

It is worth mentioning again that TP is the most suitable collection method for TEM and HRTEM analysis. It provides faster collection time and avoids sample preparation. Furthermore, it prevents contamination from other elements, as the steel from the PT, or the PTFE or fibers from the filters. Finally, the sampling grids used, allow a faster and easier process to find an appropriate zone to take the micrographs.

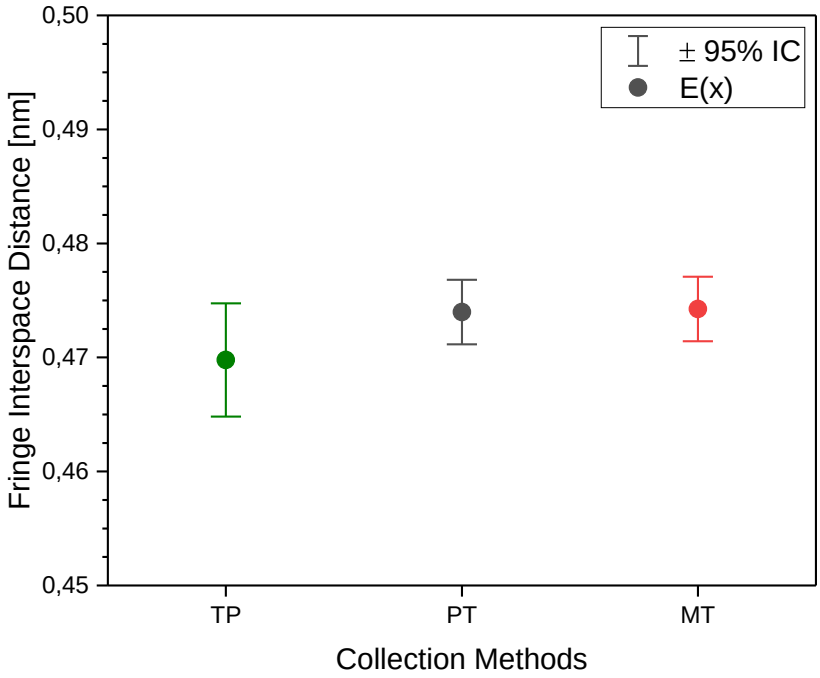

Figure 16. *Fringe interspace distance for PM of MM-B10 from HRTEM micrographs*

Figure 17 presents a typical XRD diffractogram of the PM, and Table 4 shows the results of lattice parameters determined from the deconvolution of that spectrum. The results were obtained from two different diffractograms using two powder samples from PT collection method. γ band appears around 15 of 2θ degrees, which is related to VOF content [38] or to aliphatic compounds in the PM [76]. Due to the controversy about the meaning of this band, and that it is not usually considered in the computation of lattice parameters, this band is not included in the present analysis.

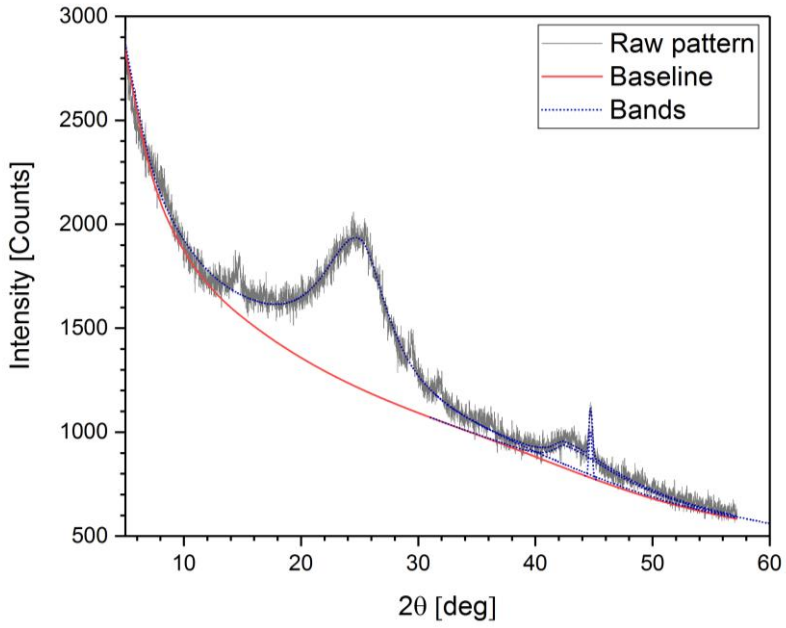

Figure 17. *Curve fitting for the XRD spectrum for PM of MM-B10 from PT*

Table 6. *Lattice parameters from XRD spectra*

	d_{002} [Å]	L_a [Å]	L_c [Å]	N [Layers]
Mean	3.60	22.95	17.03	~5
SD	0.04	1.01	5.08	-

The difference in the results of d_{002} using HRTEM or XRD can be due to differences between the analytical techniques, as stated by Cadrazco *et al.* [55]. While digital image analysis of HRTEM micrographs determines local pairs of fringes through a projected area, XRD gives a bulk measure of the average interlayer distance of the fringes in the surface of the particles. Guerrero *et al.* [72] explained that XRD peak heights are strongly influenced by the larger crystallites, being these highly ordered. Also, amorphous solid materials, such as PM, have structures characterized by a lack of periodicity where only the short-range order is kept. The result is a curve of scattered X-rays showing one or two maxima with a width that may reach 10 degrees of 2θ, as can be seen in Figure 17 for the first peak, which is used to obtain d_{002} by means of Bragg's law. On the other hand, Botero *et al.* [77] demonstrated that for mature soot particles from a diffusion flame, the fringe interspace distance decreases if it is measured in the outer side of the particle instead of the core, using HRTEM and image analysis. Figure 18 shows that the fringe interspace distance varies depending on the internal region of the particle where they are measured, and on the procedure of estimation of its value. Fringe interspace distance decreases as it moves away from the particle core towards the shell. Furthermore, a significant decrease in FS is observed when the distance between each pair of fringes is estimated when using

only the minimum pixel-pixel or using only the fringes that have fringe tortuosity less than 1.15 (almost completely flat), in contrast to when it is determined as the average of all the pixel-pixel distances. This proves that HRTEM image processing is affected by the procedure used in its estimation. For this reason, it is recommended to consider this when comparing results from scientific publications. The image processing methodology proposed by Cadrazco *et al.* [55] and used in this work, determines the average interspace distances of parallel fringes in the particle, both in the core and in the outer shell. That could explain the higher d_{002} results of HRTEM, in comparison with XRD.

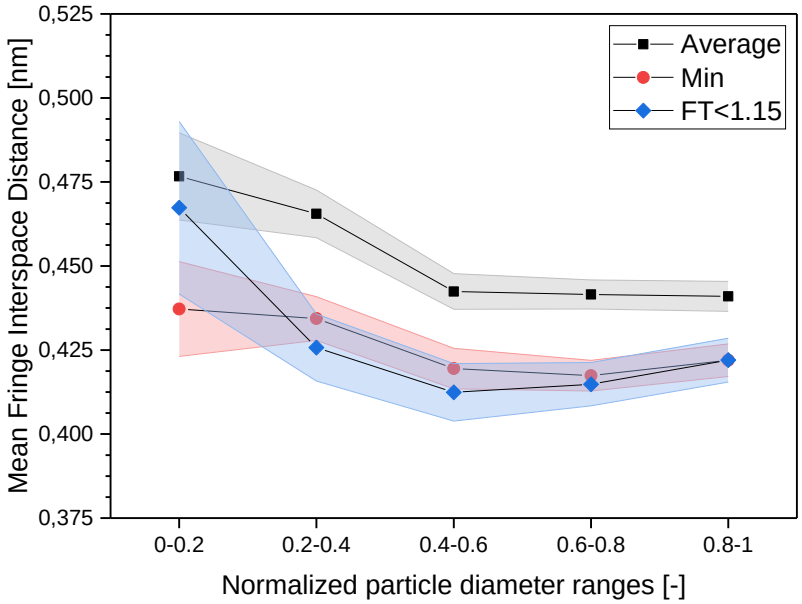

Figure 18. *Fringe interspace distances depending on the position into the particle for B10 in MM mode (Shadows are the Standard Error)*

In order to close the discussion between XRD and HRTEM results, Sharma *et al.* [78] recommend the perform the characterization of carbonaceous materials by means of HRTEM, because by means of this technique it is possible to obtain more information than from XRD, such as tortuosity and lattice parameter distributions.

On the other hand, Figure 19 shows that it is not possible to recognize the raw signal from PM collected into the filters used in MT and VP, as in the case of the Raman spectrum for the MT filter. This is due to the interference of the background support material of the filters, either fiberglass or PTFE. The result from PTFE filter (Figure 18 right) is in accordance with the study of Santos *et al.* [79], that showed the interference of the PTFE in the diffractogram, even though that the filter was highly covered by PM. Besides that, in this study it was found that the fiberglass (Figure 18 left) also affected the diffractogram,

contrary to what is reported by Santos *et al.* [79]. The fiberglass filters used by Santos e*t al.* came from atmospheric air sampling. This filters typically have a thick layer of PM on their surface. In the present study, the filters from the MT had a very thin layer, which allowed the reach of X-rays into the filtering material. Given these results, and the difficulty to collect a high amount of PM filtering the exhaust gases from current diesel engines, it is not appropriated and non-recommended to collect PM on filters for XRD experiments. Therefore, to conduct XRD analysis, it is recommended to collect PM by means of PT, due to the high amount of PM that could be collected for this method, and to the slight interference of the stainless-steel from the wools in the spectrum, which is easily identified.

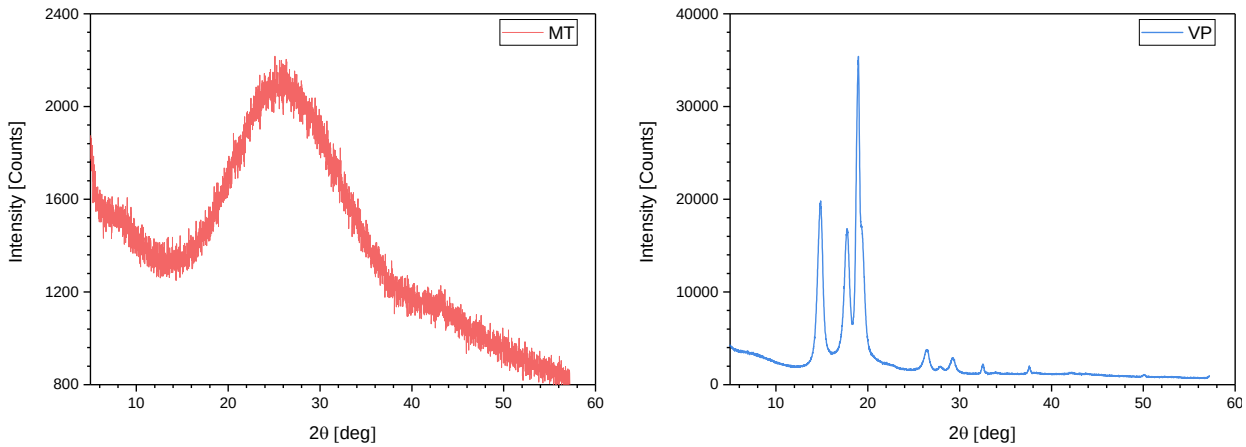

Figure 19. *Raw XRD pattern for PM at MM-B10 for MT and VP filters*

Effect of the engine operation modes and fuels

As a reminder to the reader, in this section of results only the PT and TP collection methods were used. PM from PT method was characterized by means of TGA, FTIR, Raman, and PM from TP method was characterized by means of TEM and HRTEM.

Figure 20 presents the thermogravimetric profiles of PM from both engine operating modes with both fuels, and Table 5 presents the corresponding oxidation temperatures and proximate analysis.

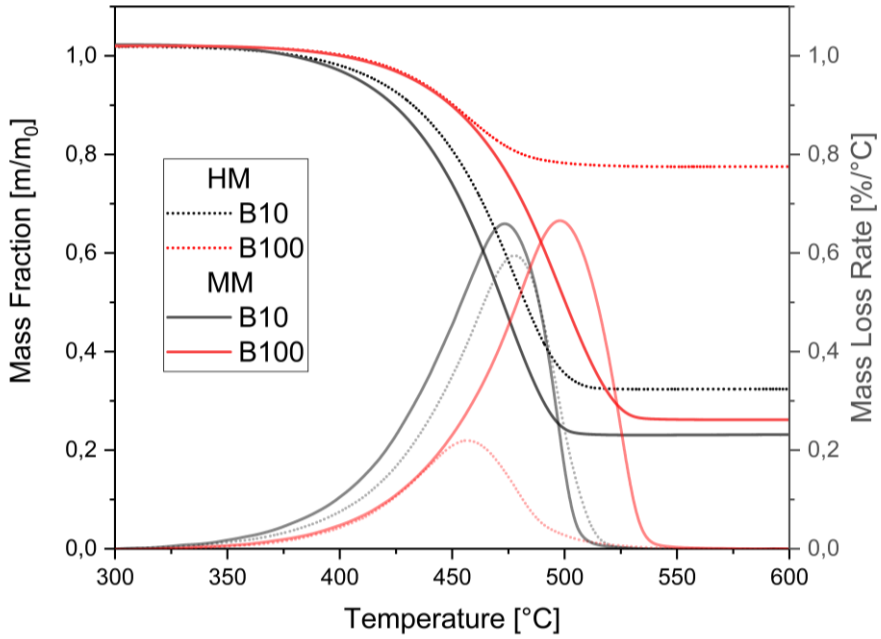

Figure 20. *Mass fraction and mass loss rate for PM from both engine operating modes with both fuels*

Information shows that PM from B10 fuel does not present large differences in $MLRT_{max}$ between both engine operating modes, although the PM from MM is slightly more reactive (4.4 °C less in $MLRT_{max}$). In contrast, B100 fuel has an opposite behavior to B10 fuel. In this case, PM from HM is more reactive than PM from MM (difference in $MLRT_{max}$ = 39.3 °C).

Table 7. *Oxidation temperatures and Proximate analysis for PM from both engine operating modes with both fuels*

Operation mode	Fuel	Oxidation Temperatures		Proximate analysis		
		$MLRT_{max}$ [°C]	$T_{10\%}$ [°C]	Ash [%]	VOF [%]	Carbon [%]
MM	B10	473.3	424.0	12.5	46.1	41.4
	B100	498.1	449.6	15.3	41.5	43.2
HM	B10	477.7	432.5	17.3	46.7	36.1
	B100	458.8	450.6	36.1	48.3	15.5

From proximate analysis, the higher ash content occurs in HM with both fuels. Furthermore, PM from HM-B100 has the highest reactivity of all samples. As can be seen in Figure A3.6, the high amount of ash in B100 soot might be due to the contamination by the stainless-steel from the wools in the PT. This could increase PM reactivity by increasing the active centers [80–82]. These images were taken with the LabRam HR Horiba microscope system.

Figure 21 shows the FT-IR peaks in the wavenumber range of 800-3600 cm^{-1}. Single bond oxigen-carbon stretch of ether C-O-C (1260 cm^{-1} [65]) is observed in the HM-B100 sample. This sample is more reactive than PM produced by B10 fuel due to its highest absorbance for the oxigenated C-O-C group [40]. On the other hand, the higher oxidation reactivity of PM from MM-B10 in regard to MM-B100 cannot be explained from FT-IR results.

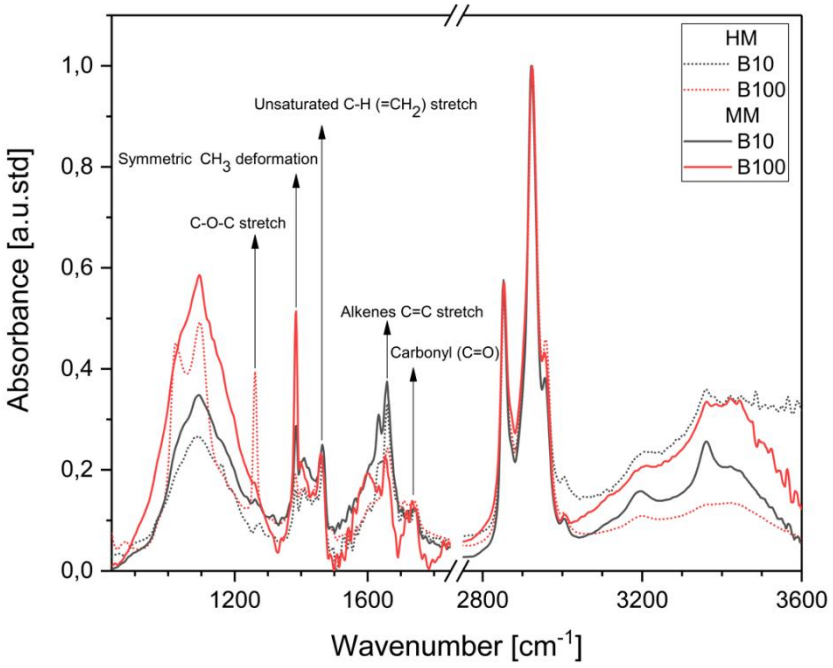

Figure 21. *FT-IR absorbance for soot samples from both engine operation modes (HM: Dark lines, MM: Dot lines)*

The area and intensity ratios of the bands of the Raman spectra are depicted in Figure 22 and 23. Is important to notice that Raman spectra for HM-B100 could not be deconvoluted, because the baseline is lost, which might be due to the previously mentioned steel contamination. For this reason, this PM sample is not shown in the figures. In MM operating mode, the increase of the oxigen content of the fuel, changing from B10 to B100, implies an increase in the degree of graphitization of PM (decrease in A_{D1}/A_G ratio). This is in agreement with the decrease in the A_{D3}/A_G ratio for PM from B100 fuel, as a result of the lower presence of amorphous carbon [37,57]. Also, Wei *et al.* [67] state that aromatics in the fuel promote the microstructure disorder, *i.e.*, the increase in I_{D1}/I_G ratio. The behavior of the PM in MM operating mode is in accordance with results obtained in several studies [67,83,84] that state that the more organized the PM, the less reactive it is.

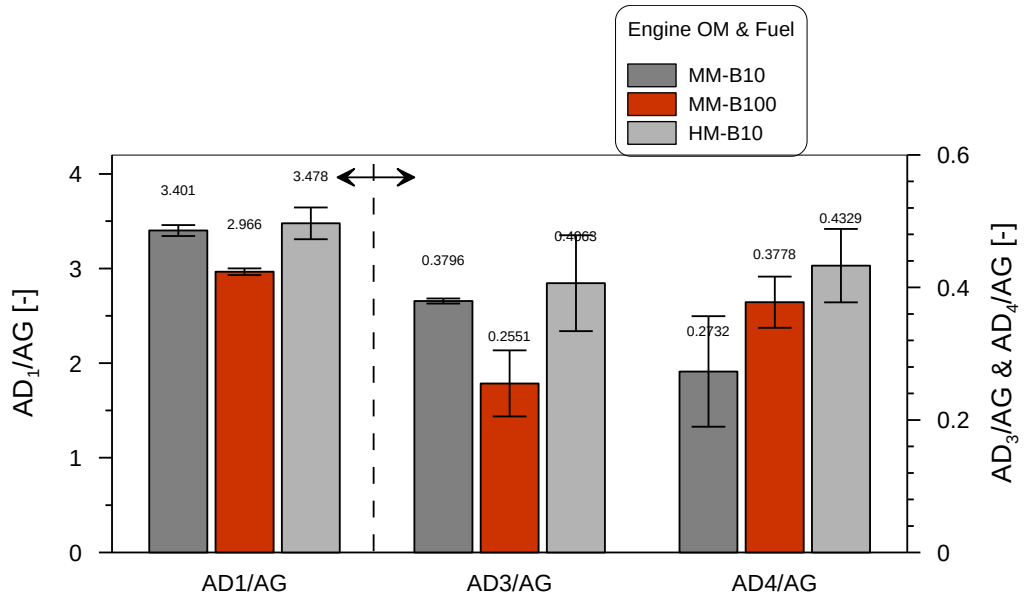

Figure 22. *Raman peak area ratios*

Xu *et al.* [68,85] found that with the increase in the engine load the order of soot nanostructural increases. In contrast, Figures 22 and 23 show that there is no significant difference in the soot nanostructure results for B10 with the increase in engine load. This behavior might be due to the small load difference between the engine operating modes used in this work. This explains the slight difference in the oxidation reactivity observed in the $MLRT_{max}$ for both PM samples.

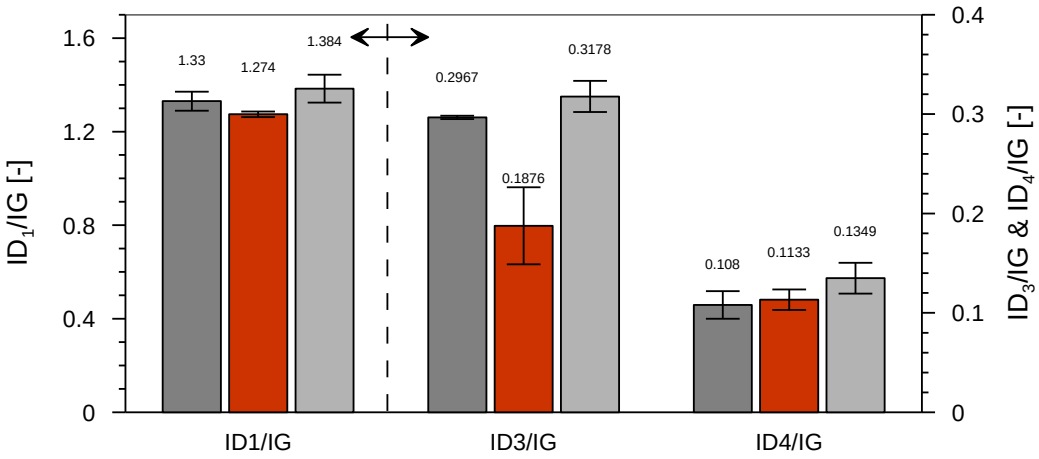

Figure 23. *Raman peak intensity ratios*

Figure 24 shows dp_0 from TEM micrographs from TP samples. This parameter decreases with the increase in fuel oxygen content, which is more noticeable in MM engine operating mode. Salamanca *et al.* [37]and Krahl *et al.* [86] demonstrated that palm oil biodiesel produces a higher number of primary particles with a diameter less than 20 nm, in contrast with diesel fuel. As Salamanca *et al.* stated, the reduction of the dp_0 was expected with B100 due to its lack of aromatics and unsaturated components. In addition, several studies conducted with oxygenated fuels present a reduction in the primary particle diameter proportional the oxygen content [87–89]. Molecular oxygen could inhibit the formation of nuclei and enhance soot oxidation during the combustion process.

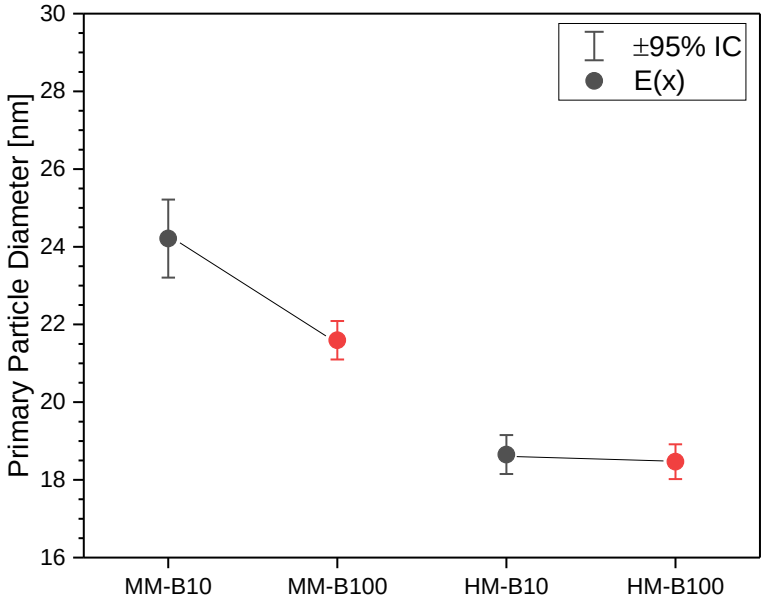

Figure 24. *Primary particle diameter for PM of both engine operation modes and both fuels tested, from TEM micrograph*

On the other hand, there is an appreciable decrease in dp_0 as a result of the increase in engine speed, due to the short in-cylinder residence time of the PM in HM, independent of the fuel used. Some studies report that increasing engine speed leads to a decrease of dp_0, because the particles have less time for surface growth [29,75,90,91]. Furthermore, that decrease is also due to the higher pressure and temperature in HM than in MM operation mode, observed in the result of the thermodynamic diagnosis (depicted in Figure A 3.3).

Figure 25 presents D_f results from TEM micrographs. Although there is not statistical difference between the results, PM from B100 tends to have a more compacted-like structure, in contrast with the structure produced by B10. This is in accordance with Merchan *et al.* [92], which found that the morphology of soot aggregates from mature soot collected in a diffusion flame becomes more complex with the increase of biodiesel in the blend. For diesel soot the morphology is more linear. Lapuerta *et al.* [71] found that the increase of engine load leads to an increase in the D_f. The results of the present study do not show a significant difference, which might be due to small load difference of the operating modes used.

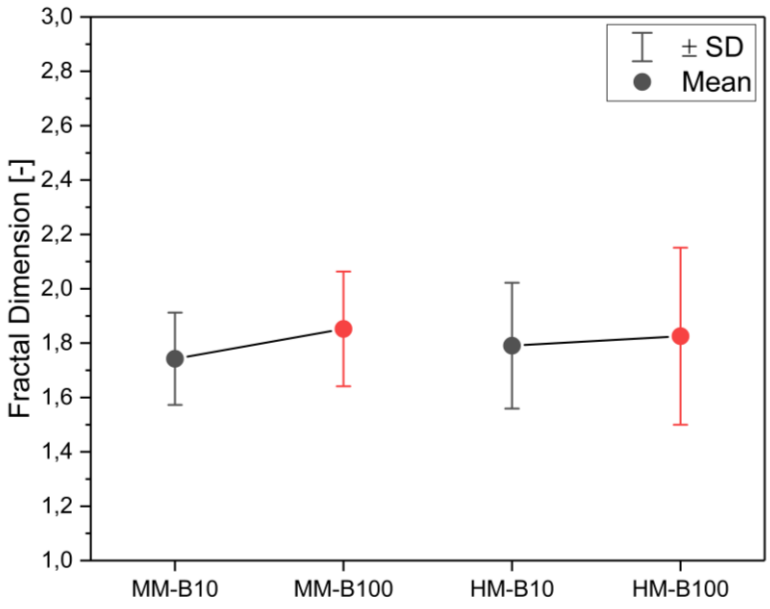

Figure 25. *Fractal dimension for PM of both engine operation modes from TEM micrographs*

Figures 26 to 28 present the nanostructural analysis from HRTEM images. Even though fringe length and fringe interspace distance results does not exhibit significant statistical differences, there is a trend to obtain lower fringe length and higher fringe interspace distance with B100 than with B10. This trend is more appreciable in MM engine operation mode, where the tortuosity is lower for PM from B10 than for B100 fuel (see Figure 28).

This result, with the previous results plotted in Figure 24, reinforces the hypothesis that lower dp_0 leads to lower fringe length and higher tortuosity in the particles, as was discussed when analyzing the effect of collection methods. This is in agreement with the trend observed for these nanostructural parameters in other investigations [54,88].

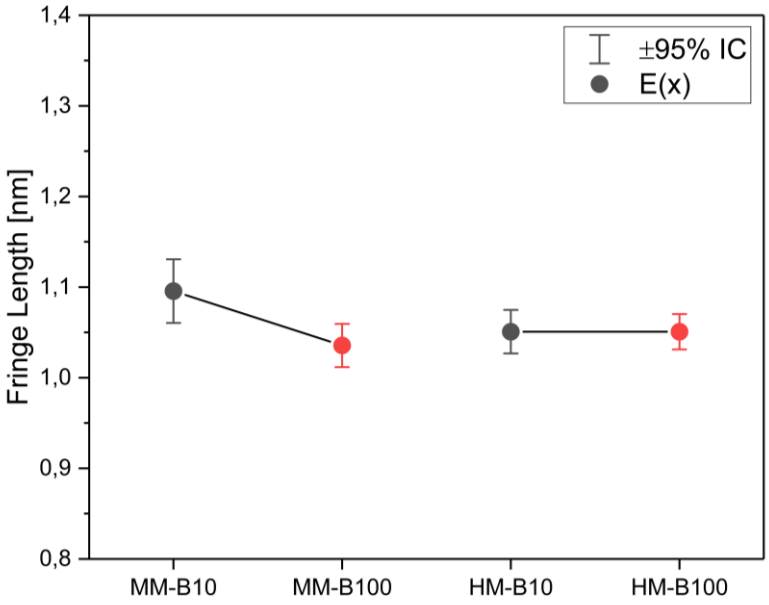

Figure 26. *Fringe length for PM of both engine operation modes from HRTEM micrographs*

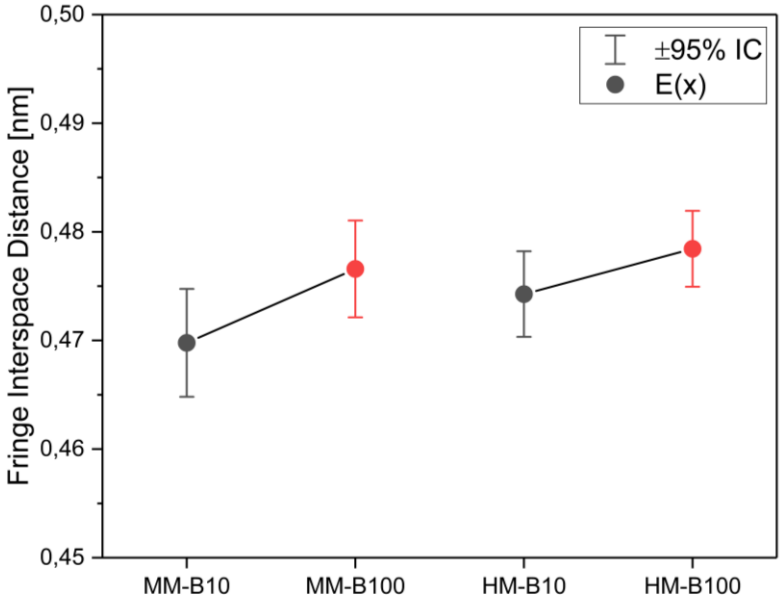

Figure 27. *Fringe spacing distance for PM of both engine operation modes from HRTEM micrographs*

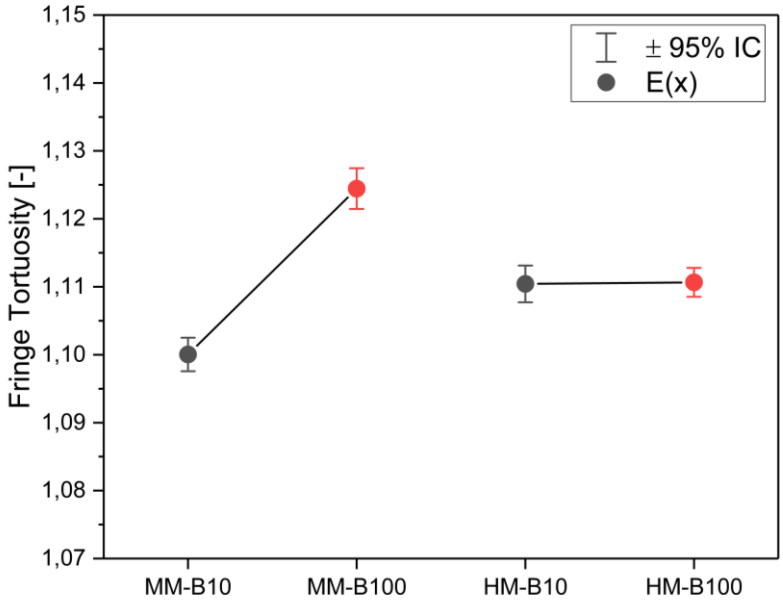

Figure 28. *Fringe tortuosity for PM of HM from HRTEM micrographs*

According to Yehliu *et al.* [84], soot from soybean oil neat biodiesel fuel presented higher fringe tortuosity and lower fringe length than that from diesel fuel. This trend is observed in Figures 26 and 28 in MM engine operating mode. Furthermore, this trend is in agreement with Liati *et al.* [69], which found that soot from rapeseed oil neat biodiesel had higher fringe tortuosity than diesel fuel. This work reports a lower fringe interspace distance for soot from neat biodiesel than from diesel fuel.

CHAPTER 4

Conclusions and future work

CONCLUSIONS AND FUTURE WORK

The main goal of this work was to determine the effect of the PM collection method in an automotive diesel engine on the results of several analytical characterization techniques. Several experiments were carried out in a Euro 4 diesel engine, installed in a steady-state test rig. Tests were performed with commercial diesel fuel (B10, a 10% v. blend of biodiesel with ULSD), at two engines operating modes. PM was collected using a thermophoretic probe (TP), a vacuum pump (VP), a particle trap (PT) and a partial dilution mini tunnel (MT). Finally, Thermo-Gravimetric Analysis (TGA), Fourier-Transform InfraRed spectroscopy (FT-IR), Transmission Electron Microscopy (TEM), X-Ray Diffraction spectroscopy (XRD), and Raman spectroscopy were conducted to determine the reactivity of PM oxidation, the functional groups in PM, and its nanostructure and morphology, respectively.

The main conclusions of this research work are presented below and briefly summarized in the next figure.

- There are significant differences in the PM mass collected by each collection method. As was expected, PT collected the higher amount of PM among collection methods.
- The characterization results are significantly affected by the PM collection method conducted.
- TP is the most appropriate method to collect PM for morphological and nanostructural analysis through TEM and HRTEM micrographs.
- On the other hand, is highly recommended to collect PM in PTFE filters by means of a VP for Raman analysis, due to its technical advantages. In addition, results suggest that this collection method does not affect the PM nanostructure and the results of Raman analysis. Nevertheless, in view of the costs associated to VP test rig, and the small statistical difference between the results of PT and VP, it is recommended to use a PT if the VP test rig is not installed.
- PT method is the most appropriate for collecting PM to determine the thermal behavior (TGA), the chemical surface groups (FT-IR), and the lattice parameters (XRD) of PM, due to the higher PM mass collected. Nevertheless, the steel contamination from the wools must be eliminated to avoid its interference in the characterization, mainly in the TGA (proximate analysis) and XRD analyses.
- Regarding the effect of fuel type and engine operating mode on PM characteristics, the greatest differences were caused by engine operating conditions. For a given fuel, the primary particle diameter decreased, and the fringe tortuosity increased when changing from mode MM to HM. This behavior might be associated with the increase in engine speed.

- For HM operating mode there were not significant differences in the nanostructure between PM from both fuels. In MM operating mode, PM from B100 fuel presented lower dp_0, which leaded to a lower fringe length and to higher fringe interspace distance and fringe tortuosity.
- Collection in MT with fiberglass filters was not suitable for the analytical techniques used in this work, given the low mass collected (bad for TGA and FT-IR) and the fluorescence that affected the Raman and XRD spectra.

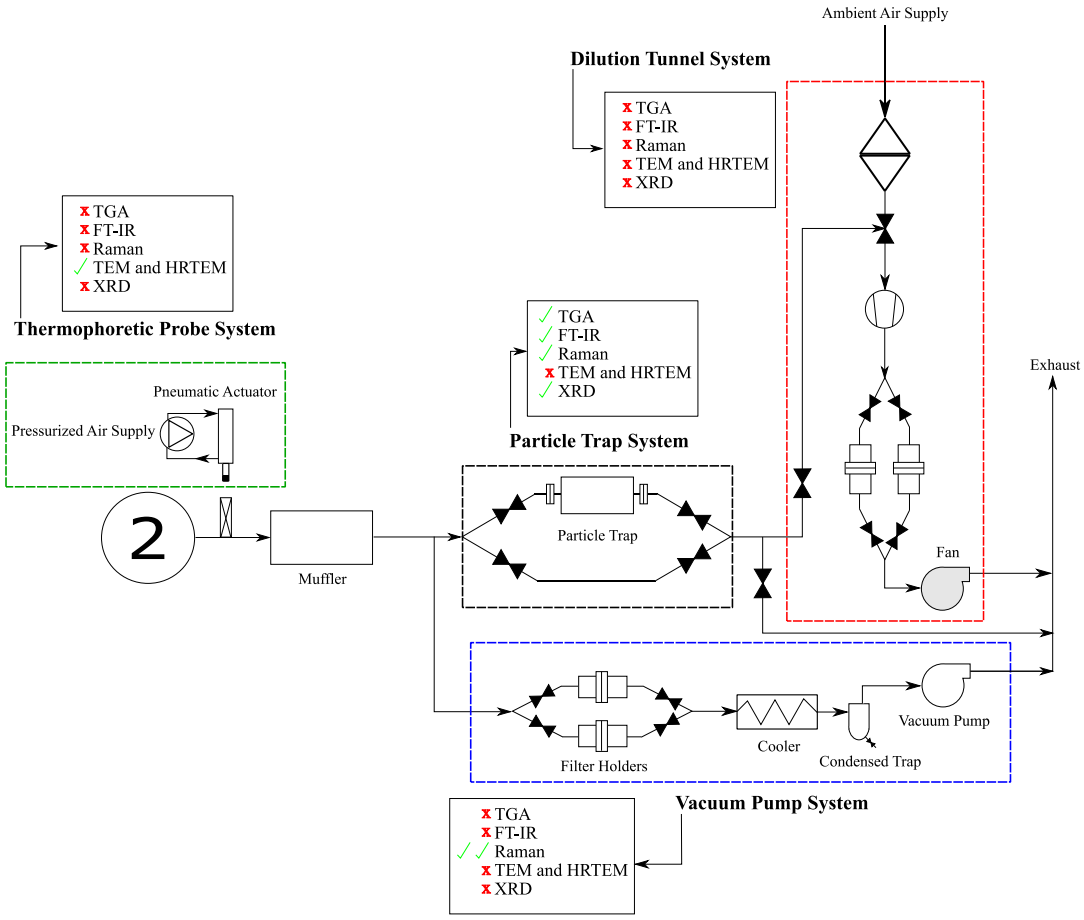

Figure 29. *Summary of the main results of this work*

As a result of the findings of the present work, the following tasks are proposed for future PM collection and characterization campaigns in steady-state engine test rigs.

- To collect high PM mass, it is proposed to use a modified non-catalyzed ceramic honeycomb particle filter. This will prevent the contamination of PM by the stainless-steel from the wools. Additionally, the collection time should be less than one hour, to avoid the possible passive oxidation, and the corresponding VOF adsorption.
- For TEM analysis (dp_0 and D_f) it is recommended to collect PM with full-film carbon grids, in order to avoid background removing for image analysis.
- For HRTEM (fringe length, fringe interspace distance and fringe tortuosity) analysis, it is recommended to collect PM with lacey carbon grids.
- To confirm the strong dependence of the results depending on the collection method used, it is recommended to extend this study to more engine operation modes and other fuels. this, using always all the collection methods of interest.
- It is recommended to explore PM collection in MT with PTFE filters, having larger collection time. This way the mass collected would increase, and the effect of dilution on PM characteristics could be determined by comparing with the results from VP filters.

REFERENCES

[1] Agarwal AK, Rajamanoharan K. Experimental investigations of performance and emissions of Karanja oil and its blends in a single cylinder agricultural diesel engine. Appl Energy 2009;86:106–12.

[2] Tse H, Leung CW, Cheung CS. Investigation on the combustion characteristics and particulate emissions from a diesel engine fueled with diesel-biodiesel-ethanol blends 2015;83.

[3] Maiboom A, Tauzia X. NOx and PM emissions reduction on an automotive HSDI Diesel engine with water-in-diesel emulsion and EGR: An experimental study. Fuel 2011;90:3179–92.

[4] Cheng CH, Cheung CS, Chan TL, Lee SC, Yao CD. Experimental investigation on the performance, gaseous and particulate emissions of a methanol fumigated diesel engine. Sci Total Environ 2008;389:115–24.

[5] Matti Maricq M. Chemical characterization of particulate emissions from diesel engines: A review. J Aerosol Sci 2007;38:1079–118.

[6] Silverman DT, Samanic CM, Lubin JH, Blair AE, Stewart PA, Vermeulen R, et al. The diesel exhaust in miners study: A nested case-control study of lung cancer and diesel exhaust. J Natl Cancer Inst 2012;104:855–68.

[7] Geng P, Yao C, Wei L, Liu J, Wang Q, Pan W, et al. Reduction of PM emissions from a heavy-duty diesel engine with diesel / methanol dual fuel Exhaust gas 2014;123:1–11.

[8] Liu Z, Ge Y, Tan J, He C, Shah AN, Ding Y, et al. Impacts of continuously regenerating trap and particle oxidation catalyst on the NO2 and particulate matter emissions emitted from diesel engine. J Environ Sci 2012;24:624–31.

[9] Mueller L, Jakobi G, Czech H, Stengel B, Orasche J, Arteaga-salas JM, et al. Characteristics and temporal evolution of particulate emissions from a ship diesel engine 2015;155:204–17.

[10] Giechaskiel B, Maricq M, Ntziachristos L, Dardiotis C, Wang X, Axmann H, et al. Review of motor vehicle particulate emissions sampling and measurement : From smoke and filter mass to particle number. J Aerosol Sci 2014;67:48–86.

[11] Zhang ZH, Cheung CS, Yao CD. Influence of fumigation methanol on the combustion and particulate emissions of a diesel engine. Fuel 2013;111:442–8.

[12] Cocker DR, Shah SD, Johnson KC, Miller JW, Norbeck JM. Development and Application of a Mobile Laboratory for Measuring Emissions from Diesel Engines. 2. Sampling for Toxics and Particulate Matter. Environ Sci Technol 2004;38:6809–16.

[13] Shah SD, Cocker DR, Miller JW, Norbeck JM. Emission Rates of Particulate Matter and Elemental and Organic Carbon from In-Use Diesel Engines. Environ Sci Technol 2004;38:2544–50.

[14] Shankar Bhavani SV, Johansson B, Andersson A. Double Compression Expansion Engine: A Parametric Study on a High-Efficiency Engine Concept. SAE Tech Pap 2018;1:1–8.

[15] Okamoto T, Uchida N. New Concept for Overcoming the Trade-Off between Thermal Efficiency , Each Loss and Exhaust Emissions in a Heavy Duty Diesel Engine. SAE Int J Engines 2016;1.

[16] Mohan B, Du J, Sim J, Roberts WL. Hydraulic characterization of high-pressure gasoline multi-hole injector. Flow Meas Instrum 2018;64:133–41.

[17] Manofsky L, Vavra J, Assanis D, Babajimopoulos A. Bridging the Gap between HCCI and SI : Spark- Assisted Compression Ignition. SAE Tech Pap 2011;1.

[18] Hyvönen J, Haraldsson G, Johansson B. Operating Conditions Using Spark Assisted HCCI Combustion During Combustion Mode Transfer to SI in a Multi-Cylinder VCR-HCCI Engine. SAE Tech Pap 2005;1.

[19] Smits M, Vanpachtenbeke F, Horemans B, De Wael K, Hauchecorne B, van Langenhove H, et al. Effect of operating and sampling conditions on the exhaust gas composition of small-scale power generators. PLoS One 2012;7:1–12.

[20] Choi SC, Roh HG, Lee KS, Lee CS. Effects of fuel injection parameters on the morphological characteristics of soot particulates and exhaust emissions from a light-duty diesel engine. Energy and Fuels 2010;24:2875–82.

[21] Ishida M, Yamamoto S, Ueki H, Sakaguchi D. Remarkable improvement of NOx-PM trade-off in a diesel engine by means of bioethanol and EGR. Energy 2010;35:4572–81.

[22] Ye P, Boehman AL. An investigation of the impact of injection strategy and biodiesel on engine NOx and particulate matter emissions with a common-rail turbocharged DI diesel engine. Fuel 2012;97:476–88.

[23] Bhaskar K, Nagarajan G, Sampath S. Optimization of FOME (fish oil methyl esters) blend and EGR (exhaust gas recirculation) for simultaneous control of NOx and particulate matter emissions in diesel engines. Energy 2013;62:224–34.

[24] Jin T, Qu L, Liu S, Gao J, Wang J, Wang F, et al. Chemical characteristics of particulate matter emitted from a heavy duty diesel engine and correlation among inorganic and PAH components. Fuel 2014;116:655–61.

[25] Mwangi JK, Lee W, Tsai J, Wu TS. Emission Reductions of Nitrogen Oxides , Particulate Matter and Polycyclic Aromatic Hydrocarbons by Using Microalgae Biodiesel , Butanol and Water in Diesel Engine. Aerosol Air Qual Res

2015;15:901–14.

[26] Chang Y-C, Lee W-J, Yang H-H, Wang L-C, Lu J-H, Tsai YI, et al. Reducing Emissions of Persistent Organic Pollutants from a Diesel Engine by Fueling with Water-Containing Butanol Diesel Blends. Environ Sci Technol 2014;48:6010–8.

[27] Zhang Z, Balasubramanian R. Physicochemical and toxicological characteristics of particulate matter emitted from a non-road diesel engine : Comparative evaluation of biodiesel-diesel and butanol-diesel blends. J Hazard Mater 2014;264:395–402.

[28] Herner JD, Hu S, Robertson WH, Huai T, Chang M-CO, Rieger P, et al. Effect of advanced aftertreatment for PM and NOx reduction on heavy-duty diesel engine ultrafine particle emissions. Environ Sci Technol 2011;45:2413–9.

[29] Chandler MF, Yingwu T, Koylu UO. Diesel engine particulate emissions: A comparison of mobility and microscopy size measurements. Proc Combust Inst 2007;31:2971–9.

[30] Wei L, Cheung CS, Ning Z. Influence of waste cooking oil biodiesel on the nanostructure and volatility of particles emitted by a direct-injection diesel engine. Aerosol Sci Technol 2016;50:893–905.

[31] Kholghy MR, Afarin Y, Sediako AD, Barba J, Lapuerta M, Chu C, et al. Comparison of multiple diagnostic techniques to study soot formation and morphology in a diffusion flame. Combust Flame 2017;176:567–583.

[32] Zhang R, Kook S. Structural evolution of soot particles during diesel combustion in a single-cylinder light-duty engine. Combust Flame 2015;162:2720–8.

[33] Al-qurashi K, Boehman AL. Impact of exhaust gas recirculation (EGR) on the oxidative reactivity of diesel engine soot. Combust Flame 2008;155:675–95.

[34] Li X, Xu Z, Guan C, Huang Z. Impact of Exhaust Gas Recirculation (EGR) on Soot Reactivity from a Diesel Engine Operating at High Load. Appl Therm Eng 2014.

[35] Rohani B, Bae C. Effect of Exhaust Gas Recirculation (EGR) and Multiple Injections on Diesel Soot Nano-structure and Reactivity. Appl Therm Eng 2016.

[36] Jung Y, Bae C. Immaturity of soot particles in exhaust gas for low temperature diesel combustion in a direct injection compression ignition engine. Fuel 2015;161:312–22.

[37] Salamanca M, Mondragon F, Agudelo JR, Santamaria A. Influence of palm oil biodiesel on the chemical and morphological characteristics of particulate matter emitted by a diesel engine. Atmos Environ 2012;62:220–7.

[38] Agudelo JR, Álvarez A, Armas O. Impact of crude vegetable oils on the

oxidation reactivity and nanostructure of diesel particulate matter. Combust Flame 2014;161:2904–15.

[39] Ruiz FA, Cadrazco M, López AF, Valdepeñas J, Agudelo JR. Impact of dual-fuel combustion with n-butanol or hydrous ethanol on the oxidation reactivity and nanostructure of diesel particulate matter. Fuel 2015;161:18–25.

[40] Soriano JA, Agudelo JR, López AF, Armas O. Oxidation reactivity and nanostructural characterization of the soot coming from farnesane - A novel diesel fuel derived from sugar cane. Carbon N Y 2017;125:516–29.

[41] Moldanová J, Fridell E, Popovicheva O, Demirdjian B, Tishkova V, Faccinetto A, et al. Characterisation of particulate matter and gaseous emissions from a large ship diesel engine. Atmos Environ 2009;43:2632–2641.

[42] Kasper A, Aufdenblatten S, Forss A, Mohr M, Burtscher H. Particulate Emissions from a Low-Speed Marine Diesel Engine. Aerosol Sci Technol 2007;41:24–32.

[43] Ouf FX, Yon J, Ausset P, Coppalle A, Maillé M. Influence of Sampling and Storage Protocol on Fractal Morphology of Soot Studied by Transmission Electron Microscopy. Aerosol Sci Technol 2010;44:1005–17.

[44] Zhu J, Lee OK, Yozgatligil A, Choi MY. Effects of engine operating conditions on morphology, microstructure, and fractal geometry of light-duty diesel engine particulates. Proc Combust Inst 2005;30:2781–9.

[45] Choi B, Jiang X. Individual hydrocarbons and particulate matter emission from a turbocharged CRDI diesel engine fueled with n -butanol/diesel blends. Fuel 2015;154:188–95.

[46] Zhang Z, Balasubramanian R. Investigation of particulate emission characteristics of a diesel engine fueled with higher alcohols/biodiesel blends. Appl Energy 2016;163:71–80.

[47] Code of Federal Regulations. Protection of the Environment, 40 CFR 86. n.d.

[48] Jiménez-palacios JL. Understanding and Quantifying Motor Vehicle Emissions with Vehicle Specific Power and TILDAS Remote Sensing. 1999.

[49] Rosenblatt P, LaMer VK. Motion of a Particle in a Temperature Gradient; Thermal Repulsion as a Radiometer Phenomenon. Phys Rev 1946;70:385–305.

[50] Lapuerta M, Ballesteros R, Rodríguez-Fernández J. Thermogravimetric analysis of diesel particulate matter. Inst Phys Publ 2007;18:650–8.

[51] Mckinnon JT, Meyer E, Howard JB. Infrared Analysis of Flame-Generated PAH Samples. Combust Flame 1996;105:161–6.

[52] Santamaría A, Mondragón F, Molina A, Marsh ND, Eddings EG, Sarofim AF. FT-IR and 1H NMR characterization of the products of an ethylene inverse

diffusion flame. Combust Flame 2006;146:52–62.

[53] Lapuerta M, Ballesteros R, Martos FJ. A method to determine the fractal dimension of diesel soot agglomerates. J Colloid Interface Sci 2006;303:149–58.

[54] Botero ML, Chen D, González-Calera S, Jefferson D, Kraft M. HRTEM evaluation of soot particles produced by the non-premixed combustion of liquid fuels. Carbon N Y 2016;96:459–73.

[55] Cadrazco M, Santamaría A, Agudelo JR. Chemical and nanostructural characteristics of the particulate matter produced by renewable diesel fuel in an automotive diesel engine. Combust Flame 2019;203:130–42.

[56] Iwashita N, Park CR, Fujimoto H, Shiraishi M, Inagaki M. Specification for a standard procedure of X-ray diffraction measurements on carbon materials. Carbon N Y 2004;42:701–14.

[57] Lapuerta M, Oliva F, Agudelo JR, Boehman AL. Effect of fuel on the soot nanostructure and consequences on loading and regeneration of diesel particulate filters. Combust Flame 2012;159:844–53.

[58] Lapuerta M, Oliva F, Agudelo JR, Stitt JP. Optimization of Raman Spectroscopy Parameters for Characterizing Soot from Different Diesel Fuels. Combust Sci Technol 2011;183:1203–20.

[59] Seong HJ, Boehman AL. Evaluation of Raman Parameters Using Visible Raman Microscopy for Soot Oxidative Reactivity. Energy & Fuels 2013;27:1613−1624.

[60] Phoungthong K, Tekasakul S, Tekasakul P, Furuuchi M. Comparison of particulate matter and polycyclic aromatic hydrocarbons in emissions from IDI-turbo diesel engine fueled by palm oil–diesel blends during long-term usage. Atmos Pollut Res 2017;8:344–50.

[61] Graboski MS, McCormick RL. Combustion of fat and vegetable oil derived fuels in diesel engines. Prog Energy Combust Sci 1998;24:125–64.

[62] Lapuerta M, Armas O, Rodríguez-Fernández J. Effect of biodiesel fuels on diesel engine emissions. Prog Energy Combust Sci 2008;34:198–223.

[63] Lapuerta M, Rodríguez-Fernández J, Sánches-Valdepeñas J, Salgado MS. Multi-Technique Analysis of Soot Reactivity from Conventional and Paraffinic diesel fuels. Flow Turbul Combust 2015.

[64] Sánchez – Valdepeñas J. Caracterización de hollín e implicaciones en la reactividad en filtros de partículas diésel. 2018.

[65] Cain JP, Gassman PL, Wang H, Laskin A. Micro-FTIR study of soot chemical composition — evidence of aliphatic hydrocarbons on nascent soot surfaces. Phys Chem Chem Phys 2010;12:5206–5218.

[66] Ishiguro T, Suzuki N, Fujitani Y, Morimoto H. Microstructural Changes of Diesel Soot During Oxidation. Combust Flame 1991;85:1–6.

[67] Wei J, Song C, Lv G, Song J, Wang L, Pang H. A comparative study of the physical properties of in-cylinder soot generated from the combustion of n -heptane and toluene/n -heptane in a diesel engine. Proc Combust Inst 2015;35:1939–46.

[68] Xu Z, Li X, Guan C, Huang Z. Effects of injection timing on exhaust particle size and nanostructure on a diesel engine at different loads. J Aerosol Sci 2014;76:28–38.

[69] Liati A, Spiteri A, Eggenschwiler PD, Vogel-Schäuble N. Microscopic investigation of soot and ash particulate matter derived from biofuel and diesel: implications for the reactivity of soot. J Nanoparticle Res 2012:1–18.

[70] Giechaskiel B, Mamakos A, Andersson J, Dilara P, Martini G, Schindler W, et al. Measurement of Automotive Nonvolatile Particle Number Emissions within the European Legislative Framework : A Review. Aerosol Sci Technol 2012;46:719–49.

[71] Lapuerta M, Ballesteros R, Martos FJ. The effect of diesel engine conditions on the size and morphology of soot particles. Int J Veh Des 2009;50:91–106.

[72] Guerrero GDJ, Raj A, Stephen S, Anjana T, Said Hammid AY, Brito JL, et al. Physicochemical properties of soot generated from toluene diffusion flames: Effects of fuel flow rate. Combust Flame 2017;178:286–96.

[73] Savic N, Rahman MM, Miljevic B, Saathoff H, Naumann KH, Leisner T, et al. Influence of biodiesel fuel composition on the morphology and microstructure of particles emitted from diesel engines. Carbon N Y 2016;104:179–89.

[74] Aso H, Matsuoka K, Sharma A, Tomita A. Structural analysis of PVC and PFA carbons prepared at 500 – 1000 ° C based on elemental composition , XRD , and HRTEM. Carbon N Y 2004;42:2963–73.

[75] Lu T, Cheung CS, Huang Z. Effects of engine operating conditions on the size and nanostructure of diesel particles. J Aerosol Sci 2012;47:27–38.

[76] Lu L, Sahajwalla V, Kong C, Harris D. Quantitative X-ray diffraction analysis and its application to various coals. Carbon N Y 2001;39:1821–33.

[77] Botero ML, Sheng Y, Akroyd J, Martin J, Dreyer JAH, Yang W, et al. Internal structure of soot particles in a diffusion flame. Carbon N Y 2019;141:635–42.

[78] Sharma A, Kyotani T, Tomita A. Comparison of structural parameters of PF carbon from XRD and HRTEM techniques. Carbon N Y 2000;38:1977–84.

[79] Santos MD, Matos JR, Carvalho LRF, Sant'Agostino LM, Korn M. An X-ray diffraction study of filters used for atmospheric aerosol sampling. Powder Diffr 1996;11:230–4.

[80] Jung H, Kittelson DB, Zachariah MR. Characteristics of SME Biodiesel-Fueled Diesel Particle Emissions and the Kinetics of Oxidation. Environ Sci Technol 2006;40:4949–55.

[81] Bhardwaj O., Lüers B, Holderbaum B, Koerfer T, Pischinger S, Honkanen M. Utilization of HVO Fuel Properties in a High Efficiency Combustion System: Part 2: Relationship of Soot Characteristics with its Oxidation Behavior in DPF. SAE Int J Fuels Lubr 2014;7.

[82] Yamane K, Asakawa T, Numao H, Komori M. Characteristics of DPF for Diesel Engine Fueled With Biodiesel Fuel - First Report : Self-Regeneration Behavior on Vehicle Road Test and Engine Bench Rig Test. SAE Tech Pap 2004;1.

[83] Vander Wal RL, Tomasek AJ. Soot oxidation: dependence upon initial nanostructure. Combust Flame 2003;134:1–9.

[84] Yehliu K, Vander Wal RL, Armas O, Boehman AL. Impact of fuel formulation on the nanostructure and reactivity of diesel soot. Combust Flame 2012;159:3597–606. doi:ddddd.

[85] Xu Z, Li X, Guan C, Huang Z. Effects of Injection Pressure on Diesel Engine Particle Physico-Chemical Properties. Aerosol Sci Technol 2013;48:37–41.

[86] Krahl J, Munack A, Schröder O, Stein H, Herbst L, Kaufmann A, et al. Fuel Design as Constructional Element with the Example of Biogenic and Fossil Diesel Fuels. Agric Eng Int 2005;VII:1–11.

[87] Hwang J, Jung Y, Bae C. Particulate morphology of waste cooking oil biodiesel and diesel in a heavy duty diesel engine. Int Conf Opt Part Charact 2014;9232.

[88] Zhang Y, Zhang R, Rao L, Kim D, Kook S. The influence of a large methyl ester on in-flame soot particle structures in a small-bore diesel engine. Fuel 2017;194:423–35.

[89] Knothe G, Sharp CA, Ryan TW. Exhaust Emissions of Biodiesel, Petrodiesel, Neat Methyl Esters, and Alkanes in a New Technology Engine. Energy & Fuels 2006;20:403–8.

[90] Lapuerta M, Martos FJ, Herreros JM. Effect of engine operating conditions on the size of primary particles composing diesel soot agglomerates. J Aerosol Sci 2007;38:455–66.

[91] Lee KO, Cole R, Sekar R, Choi MY, Kang JS, Bae CS, et al. Morphological investigation of the microsructure, dimensions, and fractal geometry of diesel particulates. Proc Combust Inst 2002;29:647–53.

[92] Merchan-merchan W, Abdihamzehkolaei A, Merchan-breuer DA. Formation and evolution of carbon particles in coflow diffusion air flames of vaporized biodiesel, diesel and biodiesel-diesel blends. Fuel 2018;226:263–77.

APPENDICES

A1. Operation manual of the vacuum pump system

Start-up

1. Ensure that one of the suction valves is open (Valves connected to the chiller end, see Figure 4).
2. Ensure that the oil level is between MIN and MAX marks.
3. Turn the top selector counterclockwise to select High flow mode. (This selector is in the vacuum pump sidewall, near the ON/OFF button).
4. Turn the selector that is above the pump to the position “II”. This allows to test with exhaust gases (See 4.2.3 section in the Manual).
5. Ensure that the chiller has water flow. For measurements without water flow (Example: on road application) fill the chiller with dry ice.
6. Turn on the vacuum pump and let idle for 15 minutes, in order to achieve the working temperature of the pump.
7. Place one filter holder with a filter on the side with the closed valve.
8. Open and close the valves in this order: First open the filter holder valve in the exhaust gas end. Second open the filter holder valve (suction side) in the chiller end. Finally, close the suction valve (open in 1).
9. Measure during the specified time.
10. Place another filter holder with a filter in the other valves side.
11. Between measurements, ensure that one flow side is always open.

Shut-Down

12. Open the valve on the side without filter (on the chiller end).
13. Turn the selector that is above the pump to the position “0”. Thus, contaminated oil recirculation is avoided.
14. Shut-down the pump with the ON/OFF button.

For maintenance, see chapter 5 of the EDWARDS’s manual (CD is in the pump’s box).

A2. Operation manual of the thermophoretic probe system

Before to start the engine and the measurements, ensure that the probe does not touch or hit into the exhaust pipe. If this happens, move the metallic base until the system is aligned.

To assure an appropriate sampling, it is recommended that the same person carry out steps 1, 2 and 11. That person must be different to the one that performs the sampling.

TEM Grid preparation

1. Clean carefully the grid holder with ethanol. Wait until all the ethanol evaporates.
2. After this, take one grid from the box with the tweezers. Place the grid on the holder and fix it with the plate and its screws.
3. Screw in the grid holder in the pneumatic actuator with the grid side up (horizontally). Now, the thermophoretic probe is ready to be transported to the sampling point.

Thermophoretic probe connection

4. Place the system into the metallic base, watching for a good fit.
5. Connect the 24V power supply with the 4 pins connector.
6. Ensure that the D7 pin led in the *Controllino*® is off.
7. Connect the airflow by means of the quick joint.
8. Open the valve fast, making sure it actuates over the switch. If the pneumatic actuator does not work, try again. If the problem persists, use the back button on the box, opening the valve fast, press the button, and when the actuator comes back, close the valve.
9. Next, disconnect the 24V power and the airflow supply, respectively.
10. Take the box to a table to remove the grid holder.
11. Remove carefully the screws and the plate. Then, use the tweezers to take the grid and place it in its slot into the box.
12. To take another grid, repeat steps from 1 to 11.

A3. Additional Information

Uncertainty analysis

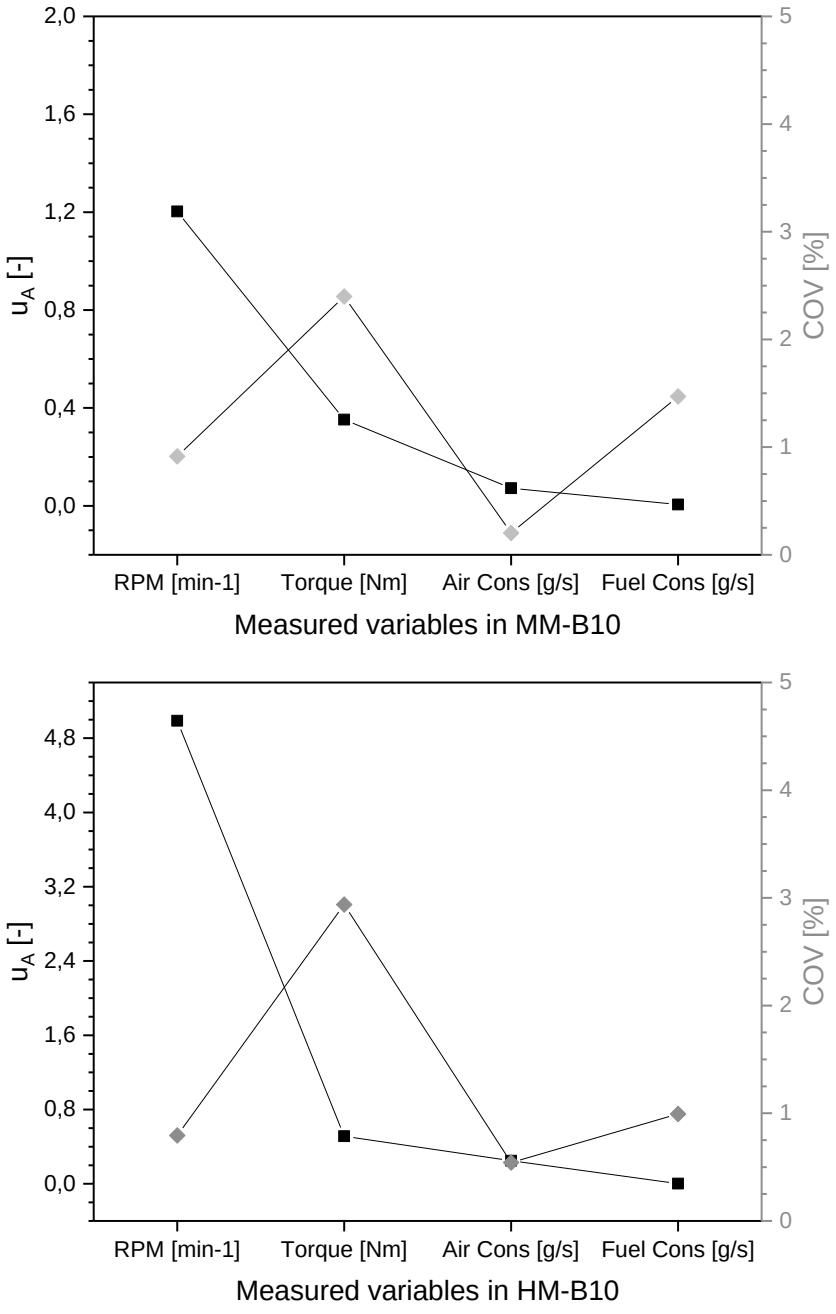

Figure A3. 1. *Uncertainty and variance coefficient analysis*

Exhaust Temperature

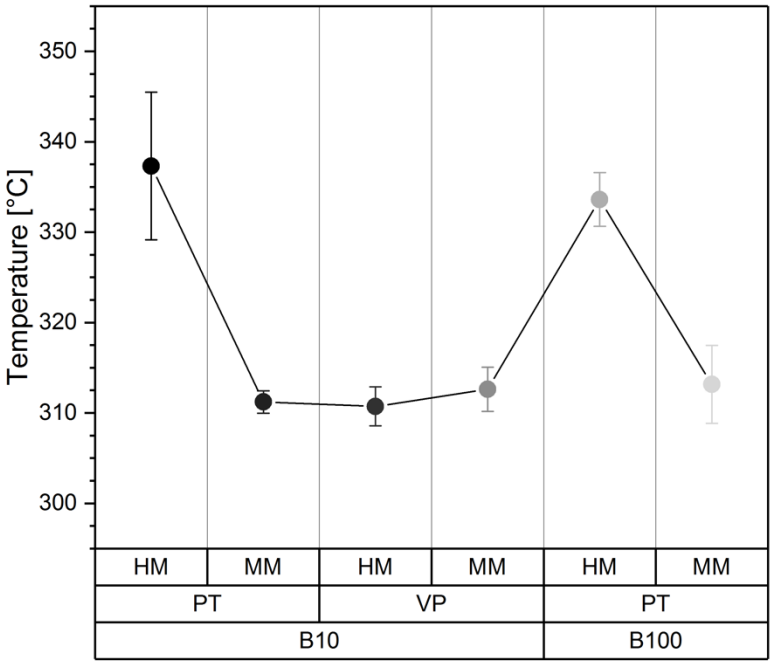

Figure A3. 2. *Exhaust gas mean temperature after turbine*

Combustion diagnosis

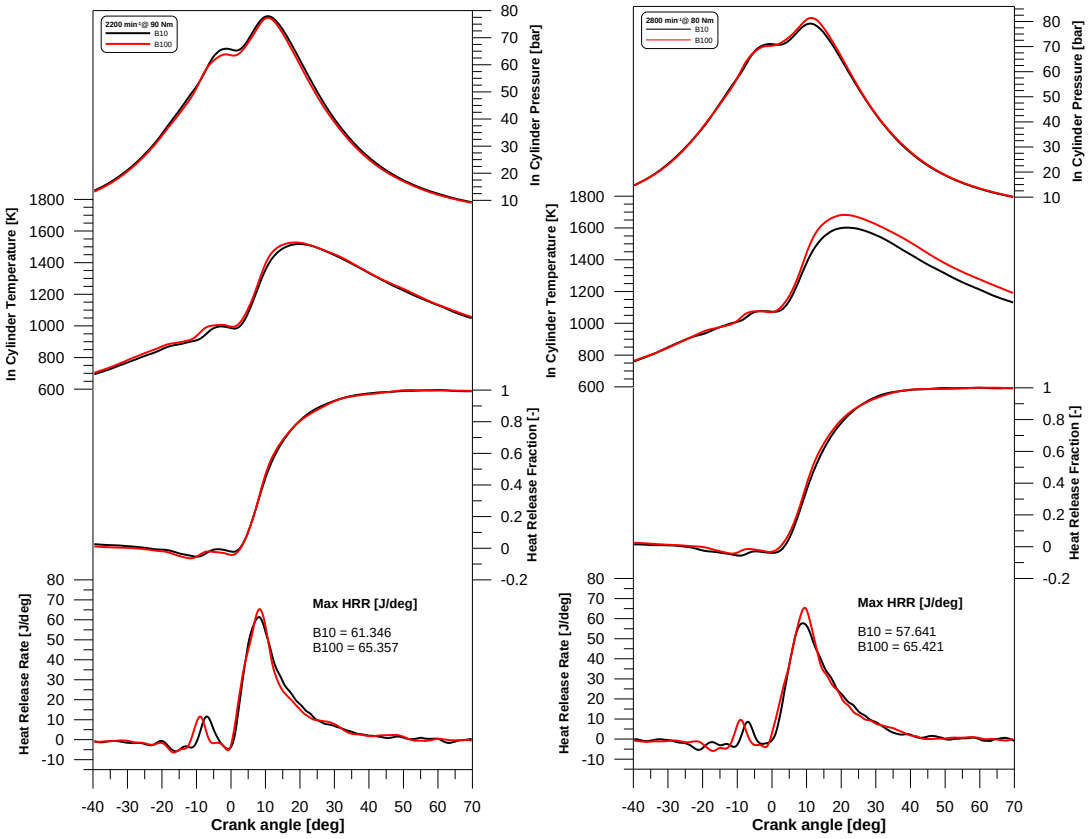

Figure A3. 3. *In-cylinder thermodynamic diagnosis of (a) MM and (b) HM engine operation modes*

TEM images: Primary particle diameter

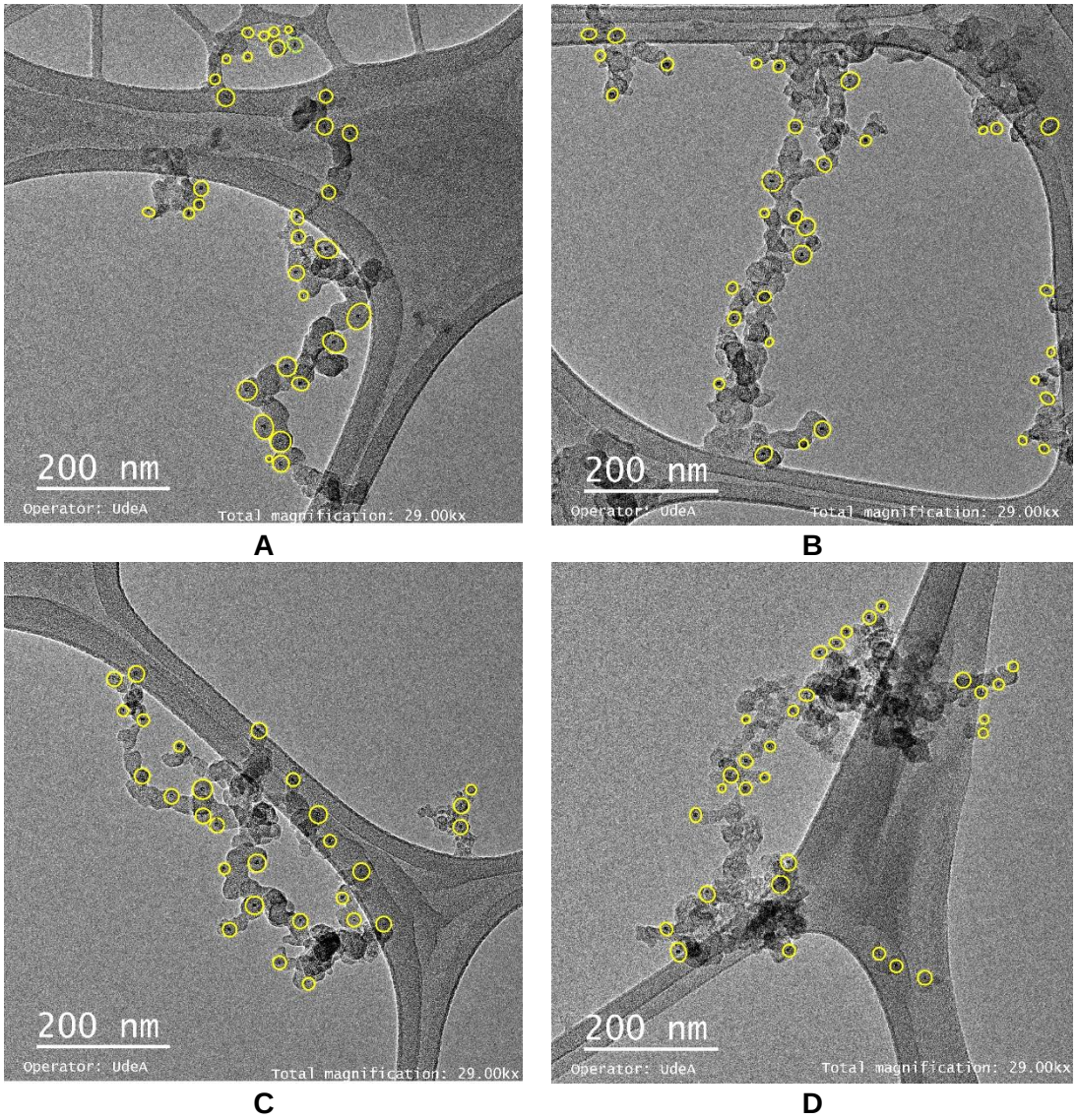

Figure A3. 4. *Illustrative TEM images of primary particle diameter measurements (**A.** MM-B10, **B.** MM-B100, **C.** HM-B10 and **D.** HM-B100)*

TEM images: Fractal dimension

MM-B10-TP

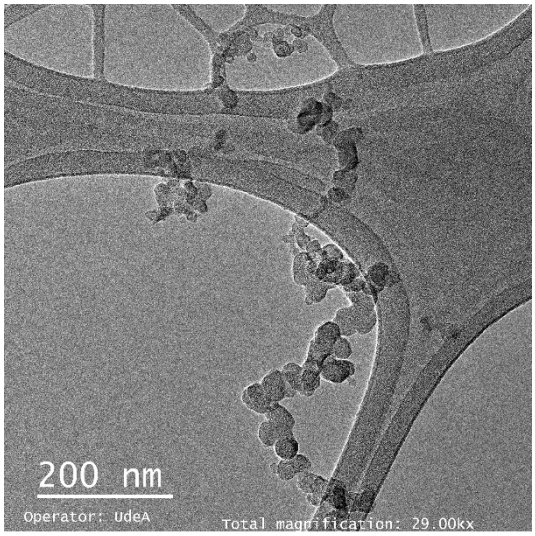

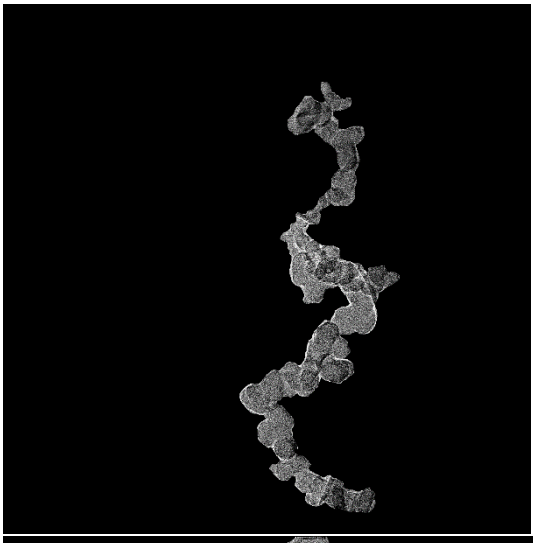

MM-B100-TP

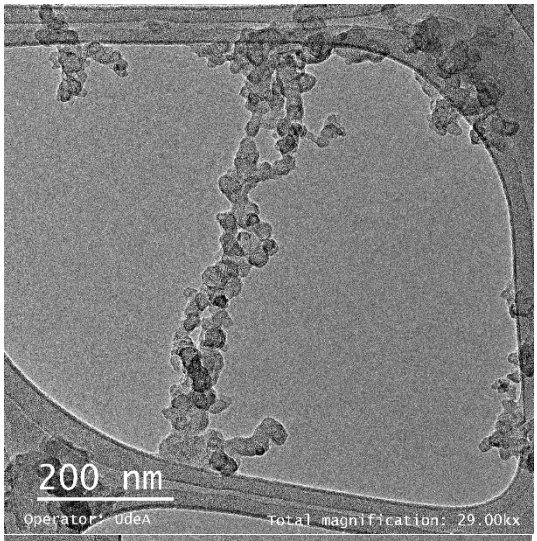

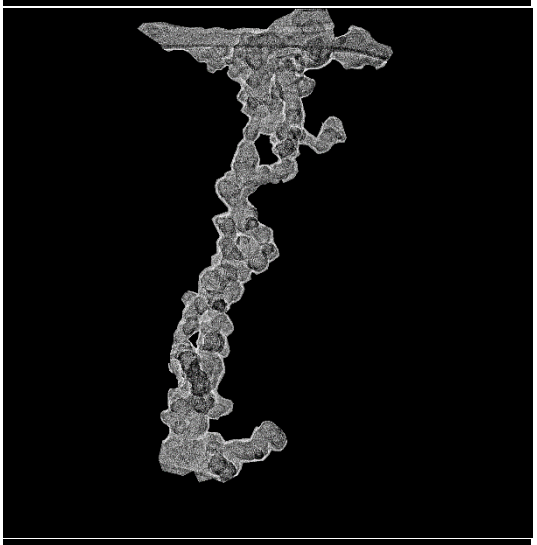

HM-B10-TP

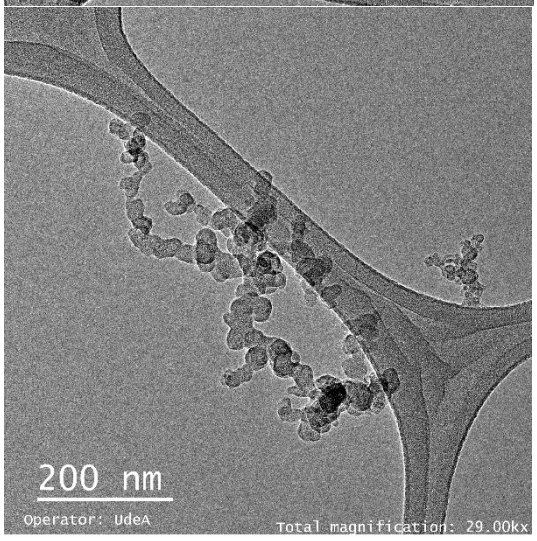

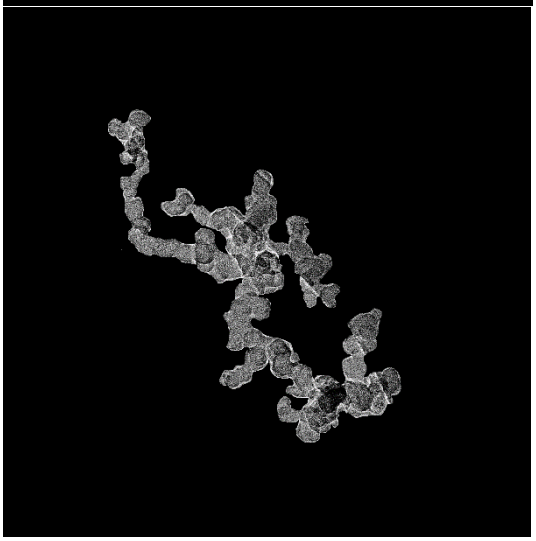

HM-B100-TP

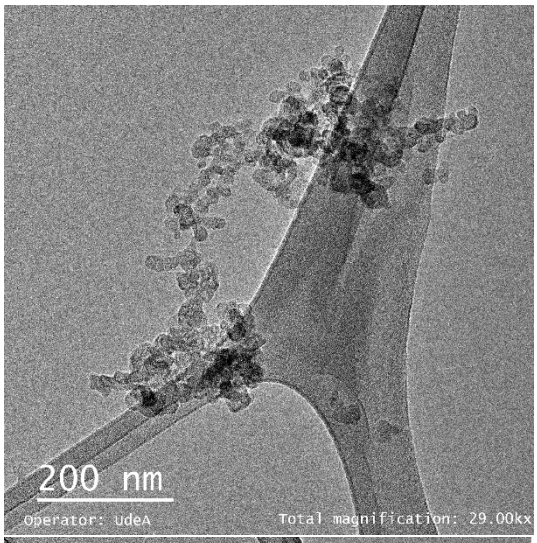

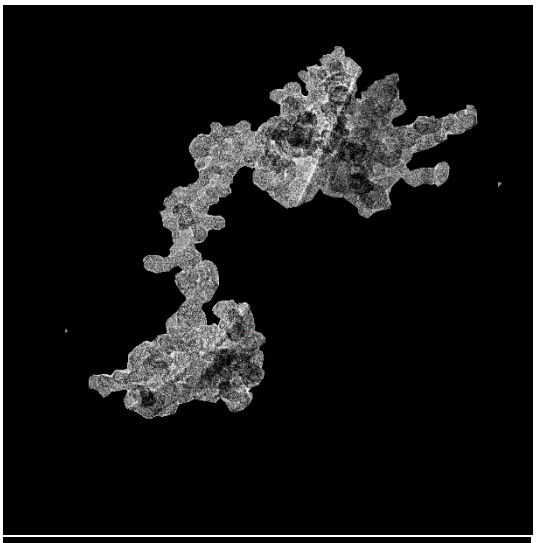

MM-B10-PT

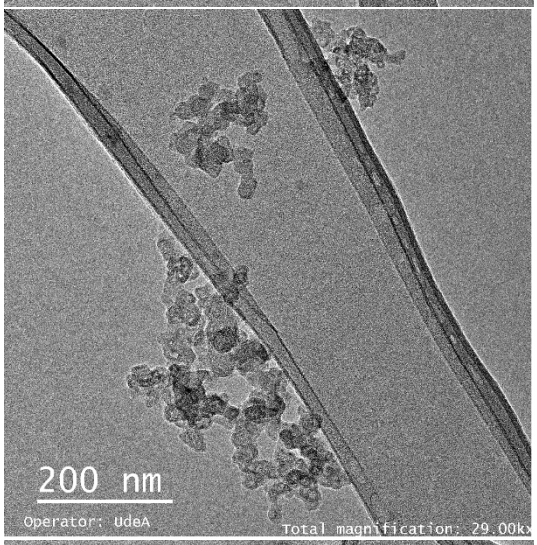

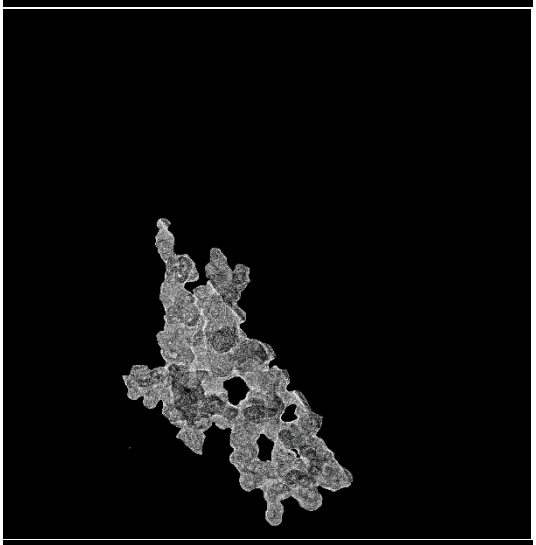

MM-B10-VP

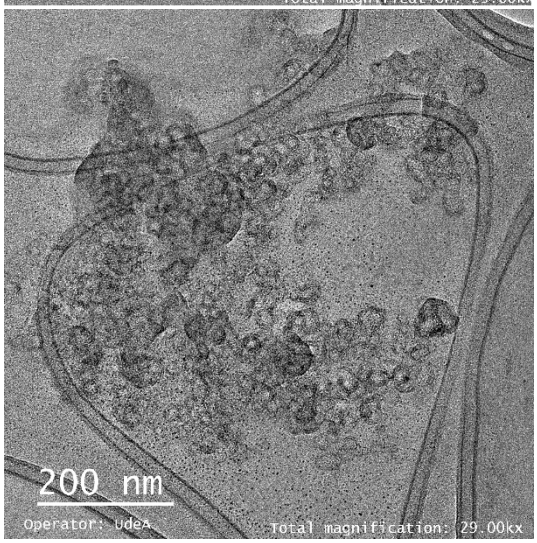

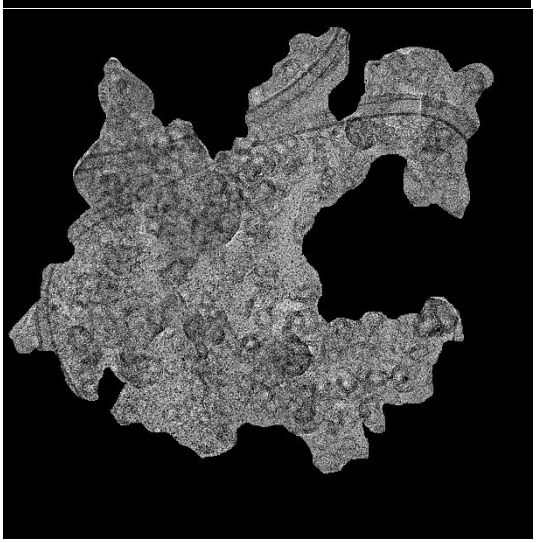

MM-B10-MT

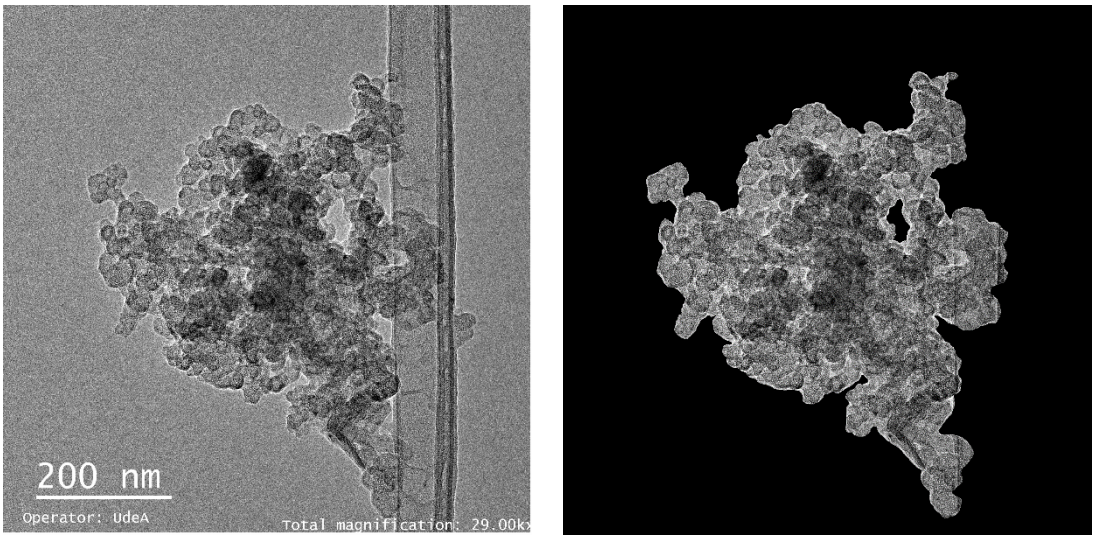

Figure A3. 5. *Illustrative TEM images for fractal dimension determination*

Stainless-steel contamination

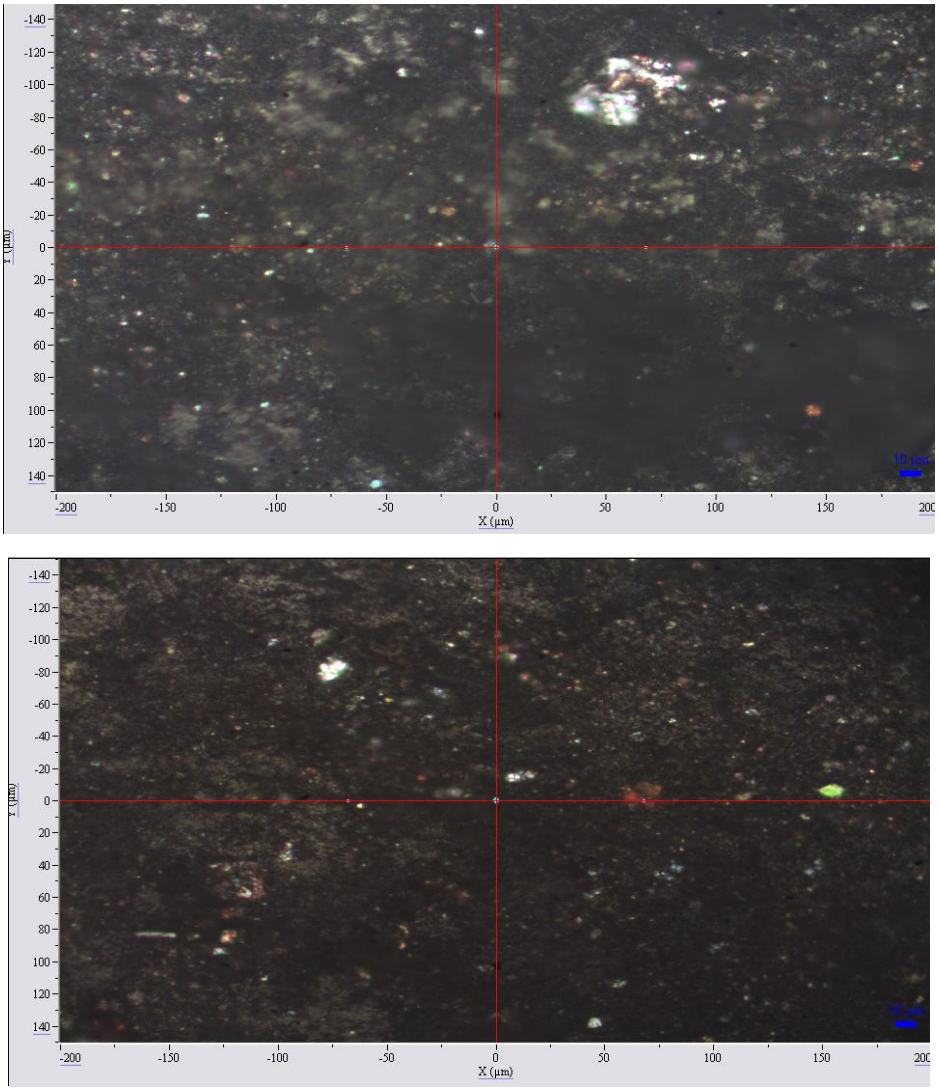

Figure A3. 6. *Soot micrographs from HM-B100*